Non-canonical Telomerase Reverse Transcriptase Controls Osteogenic Reprogramming of Aortic Valve Cells Through STAT5

Rolando A. Cuevas[1], Luis Hortells[1,2], Claire C. Chu[1], Ryan Wong[1], Alex Crane[1], Camille Boufford[1], Cailyn Regan[1], William J. Moorhead III[1], Michael J. Bashline[1], Aneesha Parwal[1], Angelina M. Parise[1], Parya Behzadi[1], Mark J. Brown[1], Aditi Gurkar[3], Dennis Bruemmer[4], John Sembrat[5], Ibrahim Sultan[6], Thomas G. Gleason[6], Marie Billaud[6], and Cynthia St. Hilaire[1,8*]

[1] Division of Cardiology, Department of Medicine, Pittsburgh Heart, Lung, Blood and Vascular Medicine Institute, University of Pittsburgh, Pittsburgh, Pennsylvania, USA.

[2] current address - Institute of Experimental and Clinical Pharmacology and Toxicology, University of Freiburg, 79110 Freiburg, Germany.

[3] Aging Institute, Division of Geriatrics, Department of Medicine, University of Pittsburgh, Pittsburgh, Pennsylvania, USA.

[4] Department of Cardiovascular Medicine, Cleveland Clinic, Cleveland, OH, USA.

[5] Division of Pulmonary, Allergy, and Critical Care Medicine, University of Pittsburgh School of Medicine, Pittsburgh, PA, USA.

[6] Division of Cardiac Surgery, Department of Cardiothoracic Surgery, Heart and Vascular Institute, University of Pittsburgh Medical Center, Pittsburgh, Pennsylvania, USA.

[7] Department of Surgery, Division of Cardiac Surgery, Brigham and Women's Hospital & Harvard Medical School, Boston, Maryland, USA.

[8] Department of Bioengineering, University of Pittsburgh, Pittsburgh, Pennsylvania, USA.

Running Title: TERT/STAT5 is required for valvular calcification

26 *Corresponding Author Contact Info:
27 Cynthia St. Hilaire, PhD, FAHA
28 University of Pittsburgh
29 BSTWR 1744.1
30 200 Lothrop Street, Pittsburgh, PA 15261
31 +1 412-648-9441 sthilair@pitt.edu

32

33 TOTAL WORD COUNT: 6617

34 ABSTRACT WORD COUNT: 268

35

36 **Background:** Calcific aortic valve disease (CAVD) is the pathological remodeling of valve
37 leaflets. The initial steps in the osteogenic reprogramming of the leaflet are not fully understood.
38 Studies have shown that TERT overexpression primes mesenchymal stem cells to differentiate
39 into osteoblasts, and we investigated whether TERT contributes to the osteogenic
40 reprogramming of valve interstitial cells (VICs).
41 **Methods:** Human control and CAVD aortic valve leaflets and patient-specific hVICs were used
42 in in vivo and in vitro calcification assays. Loss of function experiments in hVICs and cells
43 isolated from *Tert*$^{-/-}$ and *Terc*$^{-/-}$ mice were used for mechanistic studies. In silico modeling,
44 proximity ligation and co-immunoprecipitation assays defined novel TERT interacting partners.
45 Chromatin immunoprecipitation and CUT&TAG sequencing defined protein-DNA interactions.
46 **Results:** TERT protein was highly expressed in calcified valve leaflets without changes in
47 telomere length, DNA damage, or senescence markers, and these features were retained in
48 isolated primary hVICs. *TERT* expression increased with osteogenic stimuli, while knock-down
49 or genetic deletion of *TERT* prevented calcification. Mechanistically, TERT was required to
50 initiate osteogenic reprogramming independent of its canonical telomere-extending activity and

the lncRNA *TERC*. TERT exerts its osteogenic functions via binding with Signal Transducer and Activator of Transcription 5 (STAT5). Depletion and inhibition of STAT5 prevented calcification. STAT5 was found to bind the promoter region of Runt-Related Transcription Factor 2 (*RUNX2*), the master regulator of osteogenic reprogramming. Finally, we demonstrate that TERT and STAT5 are upregulated and colocalized in CAVD tissue.

Conclusions: TERT's non-canonical activity is required to initiate VIC calcification. TERT partners with STAT5 to bind the *RUNX2* gene promoter. These data identify a novel mechanism and potential therapeutic target to decrease vascular calcification.

ABBREVIATIONS:

αSMA, alpha 2 smooth muscle actin; αTUB, alpha tubulin; hVICs, human aortic valve interstitial cells; CAVD, calcific aortic valve disease; Ch-IP, chromatin immunoprecipitation; ECM, extracellular matrix; γ-H2AX, phosphorylated gamma histone 2AX; LPS, lipopolysaccharide; BMMSCs, bone marrow mesenchymal stem cells; MSCs, Mesenchymal stem cells; NT, no treatment; mVICs, mouse aortic valve interstitial cells OPN, osteopontin; OST, osteogenic treatment; PCNA, proliferating cell nuclear antigen; RUNX2, Runt-elated transcription factor 2; STAT5, Signal Transducer and Activator of Transcription 5A/B; TERC, telomerase RNA component; TERT, telomerase reverse transcriptase catalytic subunit; TL, telomere length.

Key Words:

aortic stenosis, calcific aortic valve disease, vascular calcification, osteogenic reprogramming, TERT, STAT5

Novelty and Significance

What Is Known?

76 • Calcific aortic valve disease (CAVD) is the most prevalent form of aortic valve pathology.
77 CAVD strongly correlates with age and leads to heart failure and a high risk of stroke.
78 Currently, the only therapeutic option is valve replacement, which comes with significant
79 healthcare costs and additional risks to patients.
80 • Runt-related transcription factor 2 (RUNX2) is the master transcription factor required for
81 osteogenic differentiation of stem cells to osteoblasts and osteogenic reprogramming of
82 cardiovascular cells. Yet, the early events driving its transcription in aortic valve cells are
83 poorly defined.
84 • In addition to its reverse transcriptase enzymatic activity, TERT exhibits non-canonical
85 transcriptional regulatory functions and overexpression of TERT primes mesenchymal stem
86 cells to differentiate down the osteoblast lineage.
87
88 *What New Information Does This Article Contribute?*
89 • TERT protein levels in calcified aortic leaflets and valve interstitial cells, and its non-
90 canonical osteogenic activity are independent of changes in telomere length and cell
91 senescence.
92 • Genetic loss or depletion of TERT blocks calcification in valve interstitial cells, coronary
93 smooth muscle cells, and mesenchymal stem cells.
94 • Early in the osteogenic reprogramming of VICs TERT co-localizes with STAT5, and this
95 TERT-tethered STAT5 binds to the *RUNX2* gene promoter, the master regulator of
96 osteogenic transcriptional programs.
97 • STAT5 depletion and pharmacological inhibition prevent calcification of human valve
98 interstitial cells, coronary smooth muscle cells, and mesenchymal stem cells.
99

100 *What are the clinical implications?*

101 • We have identified TERT-STAT5 as a novel signaling axis that orchestrates the early steps
102 in the osteogenic reprogramming of aortic valve cells. Inhibiting TERT and STAT5 activity, or
103 their interaction, may be leveraged to develop pharmacological or biological therapeutic
104 strategies to halt or prevent calcification in the aortic valve, bioprosthetic valves, and
105 perhaps other cardiovascular tissues.

106 • Invasive and expensive surgical procedures are currently the only treatment option for
107 patients with CAVD. The discovery and defining of the early events driving vascular
108 calcification identifies novel and druggable targets for developing non-surgical therapies.

109

110 **INTRODUCTION**

111 Calcific aortic valve disease (CAVD) encompasses a spectrum of pathological remodeling of the
112 valve leaflet, ranging from mild valve thickening that displays microcalcifications to
113 macrocalcifications that predominate in more advanced disease stages.[1,2] The advanced state,
114 aortic stenosis, results from fibrotic remodeling and the formation of calcified nodules on the
115 valve leaflet that impede and disrupt blood flow, causing excessive strain on the cardiac tissue,
116 increasing the risk of stroke and leading to heart failure.[3] CAVD severity and incidence increase
117 with age, with CAVD prevalence >1,000 per 100,000 individuals ≥75 years of age.[4,5] Further,
118 roughly 0.4-0.6% of the population harbors bicuspid aortic valve malformations, and these
119 malformed valves are prone to calcify and develop CAVD.[4] Currently, no therapeutic treatment
120 halts or reverses pathologic calcification that occurs in the aortic valve leaflets or other
121 cardiovascular tissues. The only therapeutic option to treat aortic stenosis is valve replacement
122 via surgical or transcatheter procedures, incurring substantial medical costs and health care
123 burdens to the patient.[6]
124
125 Aortic valve interstitial cells (VICs) are the primary cell type within the valve leaflet and are
126 responsible for maintaining leaflet integrity. VICs reside in a quiescent state; however, adaptive
127 or maladaptive responses to environmental factors such as inflammation, extracellular matrix
128 (ECM) breakdown, and mechanical stress may disrupt VIC homeostasis.[7,8] With alterations in
129 homeostasis, VICs acquire a myofibroblast-like phenotype, termed “activated VICs,” capable of
130 proliferation, contraction, and secretion of proteins that further remodel the extracellular milieu.[9]
131 Activated VICs can transition into calcifying cells; however, the initial steps regulating this
132 process are not fully understood. It is well established that the osteogenic reprogramming of
133 cardiovascular cells such as VICs and vascular smooth muscle cells (SMCs) is analogous to the

134 differentiation of mesenchymal stem cells (MSCs) into bone-forming osteoblasts; osteogenic
135 differentiation of MSCs and the reprogramming of cardiovascular cells is primarily orchestrated
136 by Runt-related transcription factor 2 (*RUNX2*), the master regulator of osteogenic
137 transcriptional programs.[10-12] Other osteogenic signature markers, such as osteocalcin, alkaline
138 phosphatase, and osteopontin, are upregulated in the differentiation of stem cells to osteoblasts
139 and the calcifying of VICs.[9,13] While it is accepted that VICs upregulate the expression of
140 osteogenic genes in response to stresses such as inflammation, ECM remodeling, and
141 mechanical stress, the specific mechanistic steps between those stresses and the initial
142 reprogramming events in the activation of osteogenic transcriptional reprogramming remain ill-
143 defined.
144
145 The telomerase complex extends and maintains the ends of chromosomes after cell division.
146 The core complex consists of the telomerase RNA component (*TERC*), telomerase reverse
147 transcriptase (TERT) protein, and other scaffolding proteins.[14] In addition to its role in telomere
148 maintenance, TERT also exhibits non-canonical functions independent of telomerase activity,
149 such as regulating gene expression and orchestrating chromatin remodeling.[15-17] For example,
150 TERT acts as a cofactor in Wnt-dependent promoter activation by interacting with the chromatin
151 remodeling protein SWI/SNF related, matrix associated, actin dependent regulator of chromatin,
152 subfamily a, member 4 (SMARCA4), facilitating the expression of Wnt/β-catenin target genes in
153 stem cells.[18] In a murine model of atherosclerosis, TERT induced chromatin remodeling and
154 SMC proliferation by chaperoning the retinoblastoma-associated transcription factor 1 (E2F1)
155 binding to S-phase gene promoters.[19,20] Linking together the themes of calcification and non-
156 canonical TERT, two co-published studies identified that the overexpression of *TERT* primed
157 human MSCs to differentiate down the osteogenic lineage and develop bone-like structures.[21,22]
158 The mechanism by which TERT drives the osteogenic differentiation of human MSCs is

159 unknown. Collectively, these studies provide strong evidence of telomerase-independent
160 functions of TERT in altering chromatin states and regulating gene expression via various
161 protein-protein interactions.
162
163 Signal transducers and activators of transcription (STAT) proteins play essential roles in
164 inflammatory, proliferative, and apoptotic programs, mediating the signal transduction pathways
165 of various cytokines and growth factors.[23] STATs function as transcription factors and recruit
166 chromatin remodeling and histone-modifying proteins to upregulate gene transcription.[24]
167 STAT5A and STAT5B are encoded by two highly conserved genes in humans and mice; 96% of
168 their amino acid sequence is shared, and many of their activities are redundant.[25] Herein,
169 unless specific tools utilized allow a distinction, we will refer to both generally as STAT5. Upon
170 phosphorylation, STAT5 dimerizes and translocates into the nucleus to bind the consensus
171 motif (TTCNNNGAA) and activates the promoters of various target genes by recruiting
172 transcriptional co-activators.[26,27] Furthermore, STAT5 was shown to promote the osteogenic
173 differentiation of murine MSCs.[28]
174
175 In this study, we tested the hypothesis that TERT contributes to the osteogenic reprogramming
176 of VICs. We utilized primary human aortic valve tissues from control donors and CAVD patients
177 and generated patient-specific VIC lines for in vitro disease modeling. We established baseline
178 patterns and osteogenic induction of *TERT* and calcification markers in CAVD tissue and VICs.
179 We assessed the consequences of genetic deletion or depletion of *TERT* during osteogenic
180 reprogramming in several cell types and in in vivo and ex vivo calcification models. We further
181 defined the underlying mechanism by which TERT and STAT5 participate in the osteogenic
182 reprogramming of VICs.
183

184 **METHODS**

185 **Data Availability**

186 The Materials, Methods, and Major Resources Table are found in the Supplemental Material.
187 The raw data, experimental materials, and analytic methods are available from the
188 corresponding author upon reasonable request.

189

190 **RESULTS**

191 **TERT is elevated in CAVD tissues.**

192 Human aortic valves were collected after surgical aortic valve replacement procedures or from
193 cadaveric tissue obtained via the Center for Organ Recovery and Education (CORE) of the
194 University of Pittsburgh and processed as previously described.[29] Macroscopic examination and
195 histological staining with Von Kossa were used to determine and confirm whether valves could
196 be classified as a non-calcified control or as having calcific aortic valve disease (CAVD) (**Figure**
197 **1A, Supplemental Figure 1A, Supplemental Table 1**). RUNX2 is the master transcription
198 factor required to initiate stem cells to differentiate into osteoblasts and is critical for the
199 pathological osteogenic reprogramming of vascular cells.[30-33] Immunofluorescent staining
200 showed RUNX2, and the late calcification marker OPN were significantly upregulated in CAVD
201 tissue compared to control tissues, indicating activation of osteogenic transcriptional programs
202 in CAVD tissues (**Supplemental Figure 1B**). Previous studies found that overexpression of
203 TERT primes human MSCs to differentiate down the osteogenic lineage.[21,22] We found that
204 *TERT* transcript levels were significantly upregulated in CAVD tissue relative to control samples
205 (**Figure 1B**), and *TERT* expression levels showed no correlation with the donor's age
206 (**Supplemental Figure 1C**). Markers of senescence (Cyclin Dependent Kinase Inhibitor 1A,
207 *CDKN1A*, Galactosidase Beta 1, *GLB1*), proliferation (Proliferating Cell Nuclear Antigen,

208 *PCNA*), DNA damage (Tumor Protein 53, *TP53*), and cytoskeletal markers (actin Alpha 2
209 Smooth Muscle/αSMA, *ACTA2*, Vimentin, *VIM,* interleukin 6, *IL6*) showed no statistically
210 significant differences, while the inflammatory marker and tumor necrosis factor-alpha (*TNF)*
211 was significantly elevated in CAVD samples (**Supplemental Figure 1D**), supporting
212 observations by others that indicate a role for inflammatory signaling in aortic valve calcification
213 pathogenesis.[34,35]
214
215 We detected elevated TERT protein signal in CAVD valves compared to non-calcified controls,
216 with the signal localized to areas of calcification. Similarly, the number of cells expressing TERT
217 was significantly elevated in our CAVD tissues compared to non-calcified control tissues
218 (**Figure 1C**). No statistically significant differences were observed in the staining levels of
219 proliferation marker proliferating cell nuclear antigen (PCNA) or the DNA damage indicator
220 phosphorylated gamma histone 2AX (γ-H2AX) between CAVD and control tissues
221 (**Supplemental Figure 1E**). We also found no statistically significant differences in the relative
222 mean telomere length between the control and CAVD tissues in our study (**Figure 1D**),
223 indicating no overt influence of the canonical telomere-extending functions of TERT. The mean
224 age of CAVD patients in this study was slightly elevated compared to the control patients, 68
225 and 54 years old, respectively (**Figure 1E**). Together, these data show that TERT, osteogenic
226 markers, and inflammatory signatures are upregulated in CAVD tissues compared to controls,
227 while markers indicating alterations in proliferation, DNA damage, and senescence are not
228 altered. Despite the elevated TERT expression and protein levels, telomere length remains
229 unaltered between CAVD and control tissue, suggesting non-canonical TERT activity.
230
231 **CAVD human VICs at baseline recapitulate observations in CAVD tissues.**

232 We created patient-specific valve interstitial cell (VIC) lines from CAVD and control valves.[29] At
233 baseline, freshly isolated hVICs from CAVD and control patients exhibited no morphological or
234 statistical differences in their proliferative or migratory capacity (**Figure 2, A, B, C, and**
235 **Supplemental Figure 1F**). TERT and RUNX2 proteins were significantly elevated at baseline in
236 CAVD hVICs compared to control hVICs (**Figure 2D**). We observed no statistical differences in
237 the protein levels of the hVIC activation markers SM22 or alpha SMA between CAVD and
238 control hVICs but observed a significant increase of the mineralizing enzyme tissue non-specific
239 alkaline phosphatase (TNAP) in CAVD hVICs (**Supplemental 1G**). Like in the leaflets, there
240 was no statistical difference in the relative telomere length between CAVD and control hVICs
241 (**Figure 2E**). These data show that hVICs isolated from CAVD patients display elevated TERT
242 and RUNX2 expression compared to non-calcified control hVICs, recapitulating the osteogenic
243 phenotype observed in CAVD leaflet tissue.
244
245 **TERT expression is upregulated in human VICs in an in vitro osteogenic disease model.**
246 To model CAVD in vitro and establish a role for TERT during hVIC osteogenic reprogramming,
247 we cultured CAVD and control hVICs in osteogenic media conditions (OST), a media widely
248 utilized to induce osteogenic differentiation of stem cells to osteoblasts.[36] Alizarin Red staining
249 for calcification revealed that both OST-treated CAVD and control hVICs lay down calcified
250 matrix as early as 14 days (d14), CAVD hVICs calcified earlier relative to control hVICs (**Figure**
251 **2F**). Importantly, we observed that CAVD hVICs calcify de novo under no treatment (NT)
252 conditions, suggesting that CAVD hVICs are primed for osteogenic reprogramming (**Figure 2F**).
253 TERT protein levels were significantly increased in control hVICs after d14 of OST treatment,
254 while in CAVD hVICs, TERT was elevated even under NT conditions (**Figure 2G**). The
255 calcification markers RUNX2 and OPN were significantly upregulated, indicating active
256 osteogenic reprogramming (**Figure 2G**). TERT protein signal was elevated in CAVD hVICs

257 relative to control hVICs at d14 under NT conditions (**Figure 2H**, left panels). At d14 of OST, the
258 TERT protein staining was elevated and localized near areas of calcification in both control and
259 CAVD hVICs; however, CAVD hVICs formed larger calcified nodules (**Figure 2H**, right panels).
260 We observed no significant differences in cell numbers at the end of the 14-day assay under NT
261 or OST treatment conditions (**Supplemental Figure 2A**). As CAVD hVICs exhibit elevated
262 osteogenic markers at baseline (**Supplemental Figure 1G**) and are prone to calcify (**Figure 2H**)
263 de novo, we assessed transcripts in control hVICs under OST. Osteogenic markers *BMP2*,
264 *THBS1*, *ALPL,* and myofibroblast markers *CNN1*, *TAGLN*, and *SMTN* were significantly
265 upregulated in control hVICs at d14 of OST treatment (**Figure 2I**). Likewise, the calcification-
266 associated gene *FOXO1* and the CAVD-associated metalloproteinase *MMP13* were also
267 significantly upregulated in OST conditions, as shown previously.[37,38] Lastly, the pro-
268 inflammatory transcription factor Signal Transducer and Activator of Transcription 5A *(STAT5A)*
269 was significantly upregulated, while the expression of the isoform *STAT5B* remained
270 unchanged. These results show that hVICs undergo osteogenic reprogramming instead of de
271 novo mineral nucleation.[39]
272
273 In cancer and stem cells, elevated expression of TERT is associated with long telomeres and
274 enables unlimited proliferation, while short telomeres can trigger cellular senescence.[40,41]
275 Although we observed no differences in telomere length in our tissues and cells in this study
276 (Figures 1D and 2E), we assessed cellular senescence and observed no significant differences
277 in the expression of senescence-associated β-galactosidase (SA-β-gal, *GLB1*) between CAVD
278 and control hVICs at baseline **(Supplemental Figure 2B)** nor increased in control hVICs in OST
279 treatment (**Figure 2I**). SA-β-gal activity staining indicated that cellular senescence was not
280 engaged even after 28 days of OST treatment (**Supplemental Figure 2C**). These data
281 confirmed that cellular senescence is not operative during hVICs osteogenic reprogramming.

282

283 **TERT is required for the osteogenic differentiation of human MSCs.**

284 Previous studies have shown that the overexpression of TERT primes human mesenchymal
285 stem cells (hMSCs) to differentiate into osteoblasts.[21,22] To assess the role of endogenous
286 TERT in osteogenic differentiation, we subjected hMSCs to NT and OST treatment. OST
287 treatment induced robust calcification as early as day 14, while cells in NT conditions did not
288 calcify (**Supplemental Figure 3A**). Protein analysis showed that the TERT protein levels
289 significantly increased on day 3 of the OST treatment, coinciding with increased *RUNX2*
290 expression and RUNX2 protein levels (**Supplemental Figures 3B and 3C**). hMSCs in OST
291 treatment exhibited intense TERT staining, and TERT-positive cells clustered around calcified
292 nodules (**Supplemental Figure 3D**). Using lentiviral-mediated transduction of expressing short-
293 hairpin RNA to deplete TERT (shTERT) or scrambled control (shControl), we found that
294 knockdown of *TERT* significantly inhibited the calcification of hMSCs (**Supplemental Figures**
295 **3E and 3F**). While previous studies show that overexpression of *TERT* primed hMSCs to
296 undergo osteogenic differentiation, our data show that TERT is required for the osteogenic
297 differentiation of hMSCs.[21,22]

298

299 **TERT is required for calcification in vitro and in vivo.**

300 Control hVICs were transduced with shControl and shTERT lentivirus, and like hMSCs,
301 knockdown of *TERT* significantly inhibited calcification compared to the control group and
302 downregulated RUNX2 protein levels (**Figures 3A and 3B**). We assessed TERT's role in
303 calcifying human coronary artery smooth muscle cells (hCASMCs), which calcify in
304 atherosclerotic plaques.[42] Knocking down TERT significantly inhibited hCASMCs calcification
305 (**Figure 3C**). Together, these data indicate that TERT is essential for the osteogenic
306 reprogramming of hVICs and hCASMCs. Next, mice VIC (mVICs) and bone marrow MSCs

307 (mBMMSCs) lines were generated from *Tert*$^{+/+}$ and *Tert*$^{-/-}$ mice.[43] In line with our observations in
308 human cells with depleted TERT, we observed significant inhibition of calcification in *Tert*$^{-/-}$
309 mVICs (**Figure 3D**) and *Tert*$^{-/-}$ mBMMSCs (**Supplemental Figure 4A**) compared to *Tert*$^{+/+}$ cells.
310 No statistically significant differences were observed in senescence-associated β-galactosidase
311 activity in mVICs or mBMMSCs (**Supplemental Figures 4B** and **4C**).
312
313 To determine whether TERT is required to initiate and/or maintain osteogenic reprogramming,
314 we cultured control hVICs in OST and transduced shTERT lentivirus 7 or 14 days later, and
315 calcification was assessed at day 21. Control hVICs transduced with shTERT on day 7 showed
316 a significant reduction in calcification compared to the OST alone, while transduction of shTERT
317 on day 14 did not show any decrease in calcification (**Supplemental Figure 4D**), indicating that
318 TERT is required to initiate reprogramming to the osteogenic phenotype.
319
320 Next, we used *Tert*$^{+/+}$ and *Tert*$^{-/-}$ mice to test whether Tert is required for diet-induced non-
321 atherosclerotic medial arterial calcification in vivo. Of note, *Tert*$^{-/-}$ mice were generated from
322 heterozygous breeding pairs (F1 generation) and thus did not exhibit shortened telomeres.[44]
323 *Tert*$^{+/+}$ and *Tert*$^{-/-}$ mice were fed the A6P6 diet, which was previously shown to induce medial
324 arterial calcification in the vasculature of mice.[45] At the end of the 12-week regime, we observed
325 significantly higher levels of calcification in the aorta of *Tert*$^{+/+}$ compared to *Tert*$^{-/-}$ mice (**Figure**
326 **3E**). Staining for Runx2 protein mirrored calcification presentation and was significantly higher in
327 the *Tert*$^{+/+}$ compared to *Tert*$^{-/-}$ tissue (**Figure 3F**). These findings were validated in an ex vivo
328 calcification assay. Thoracic aortic rings obtained from the *Tert*$^{+/+}$ and *Tert*$^{-/-}$ mice were cultured
329 in ex vivo OST or control NT medium for 14 days. *Tert*$^{+/+}$ aortic rings exhibited significantly
330 elevated calcification compared to aortic rings from *Tert*$^{-/-}$ mice (**Supplemental Figure 4E**).
331 *Tert*$^{+/+}$ aortic rings also exhibited prominent staining for Runx2 protein, which was absent in

332 aortic rings from *Tert*$^{-/-}$ mice (**Supplemental Figure 4F**), and western blot analysis confirmed
333 elevated Runx2 protein levels in *Tert*$^{+/+}$ aortic rings compared to *Tert*$^{-/-}$ (**Supplemental Figure**
334 **4G**). Neither calcification nor Runx2 was detected in the NT groups. Together, these data show
335 that TERT is required for osteogenic reprogramming of cells in vitro and in vivo.
336
337 TERT's canonical telomere-extending activity requires the telomerase RNA component (*Terc*) to
338 maintain chromosome telomere length and genome integrity.[14] *Terc* exerts a dual function in the
339 telomerase complex; it guides the telomerase complex to the telomere ends and serves as the
340 primer for TERTs reverse transcriptase activity, *Terc* also is a scaffold that tethers the additional
341 proteins of the telomerase complex (i.e., Dyskerin, NOP10, GAR1 and NHP2).[46] *Terc* is
342 essential for the canonical telomere-extending activity of TERT.[47] To ensure that TERT's role in
343 calcification is independent of its telomere-extending function, we isolated mVICs from *Terc*$^{-/-}$
344 mice. While *Tert*$^{-/-}$ mVICs did not calcify under OST conditions, *Terc*$^{-/-}$ mVICs were significantly
345 calcified (**Figure 3G**). Similarly, in hVICs, BIBR1532, which blocks the reverse transcriptase
346 activity of TERT,[48] did not prevent calcification nor decrease the expression of *RUNX2*
347 (**Supplemental Figure 4H and 4I**). Together, these data illustrate that the canonical telomere-
348 extending function of TERT does not contribute to osteogenic reprogramming.
349
350 **TERT/STAT5 interact and bind to the *RUNX2* gene promoter to initiate osteogenic**
351 **reprogramming.**
352 Several studies have shown that TERT participates in gene transcription by physically
353 interacting with transcription factors.[17,20,49,50] RUNX2 is the master regulator of osteogenic
354 differentiation of stem cells.[30,31] Increased *RUNX2* expression and transcriptional activity are the
355 hallmarks of osteoblast differentiation and cardiovascular calcification and are required for

356 osteogenic reprogramming of vascular cells.[32,33] As our data show that RUNX2 is significantly
357 downregulated in *TERT*-knockdown and deficient cells (Figure 3), we used the LASAGNA[51] and
358 TRANSFAC/MATCH[52] programs to identify putative transcription factor binding sites in the 5 kb
359 region upstream of the human *RUNX2* gene promoter (NM_001015051.3) and identified eight
360 potential STAT5 binding sites (**Supplemental Table 2**). We sought to determine whether
361 STAT5 is bound to the *RUNX2* gene promoter and focused on the two most proximal predicted
362 STAT5 sites located at -1371 bp and -193 bp upstream of the transcriptional start site (TSS), as
363 both have high homology to the tetrameric consensus STAT5 binding site and show an elevated
364 likelihood of being functional sites (**Figures 4A** and **4B**). As inflammation and inflammatory
365 signaling pathways are known to contribute to CAVD pathogenesis[1,53], we used bacterial
366 lipopolysaccharide (LPS) as a broad method to activate inflammatory response pathways in
367 hVICs. We found that LPS was sufficient to induce calcification of hVICs and that TERT-positive
368 cells accumulated near calcified nodules (**Figure 4C**). Protein analysis showed that OST and
369 LPS significantly upregulate TERT, RUNX2, and STAT5 proteins (**Figure 4D**). TERT protein
370 levels were elevated in both the cytosol and nucleus of cells upon OST stimulation
371 (**Supplemental Figure 5A**). Under NT conditions, STAT5 is observed in the membrane and
372 cytosol but translocates and accumulates in the nucleus of hVICs in OST (**Supplemental**
373 **Figure 5B**). Next, we used genetic and pharmacological approaches to determine the
374 requirement of STAT5 for the calcification of hVICs. The small molecules StafiA-1 and StafiB-1
375 specifically inhibit STAT5A and STAT5B, respectively.[54,55] We found that StafiA-1 significantly
376 inhibited calcification of control hVICs during a 21-day OST assay and that this inhibition was of
377 a greater extent than the inhibition observed when control hVICs were treated with StafiB-1,
378 suggesting that STAT5A is the main participant during the osteogenic reprogramming of hVICs
379 (**Figure 4E**). StafiA-1 significantly reduced calcification in hCASMCs and hMSCs
380 (**Supplemental Figures 5C** and **5D**). Lentiviral-mediated delivery of shControl or shSTAT5

381 constructs showed that knocking down STAT5 significantly attenuated calcification (**Figure 4F**),
382 confirming an essential role for STAT5 in the osteogenic reprogramming of hVICs. Knocking
383 down STAT5 after 7 or 14 days of OST treatment did not reduce calcification (**Figure 4G**),
384 indicating that STAT5 activity is required during the initial steps of osteogenic reprogramming.
385 Others have established that TERT can interact with transcription factors to regulate gene
386 expression.[17,20,49,50] We assessed whether TERT and STAT5 directly interact. Three methods
387 were utilized: proximity ligation assay (PLA), co-immunoprecipitation (IP), and exogenously
388 expressing TERT and STAT5 reporters. PLA can detect protein-protein proximity <40 nm
389 apart.[56] PLA revealed that OST significantly increased TERT and STAT5 colocalization in
390 control hVICs after 21 days of OST treatment relative to NT condition (**Figure 4H**). Focusing
391 only on nuclear co-localization, TERT/STAT5 puncta are significantly elevated in the nucleus of
392 calcifying hVICs relative to the NT condition (**Supplementary Figure 5E**). Protein IP also shows
393 that TERT and STAT5 physically interact in hVICs upon OST treatment relative to NT condition
394 (**Figure 4I**). These data show that TERT and STAT5 interact and translocate into the nucleus
395 during the osteogenic reprogramming of hVICs. Supporting a role for STAT5 in osteogenic
396 reprogramming, STAT5 protein levels were significantly lower in the aorta of *Tert*$^{-/-}$ mice fed the
397 A6P6 diet compared to the aorta from *Tert*$^{+/+}$ mice (**Supplemental Figures 5F**), and these
398 findings were replicated in the ex vivo calcification assay (**Supplemental Figure 5G**). While the
399 domains of TERT were initially defined by their role in the telomere-extending functions of
400 TERT, protein partners required for the known non-canonical functions of TERT have been
401 found in several domains throughout the protein.[57] Further, sites for protein binding partners to
402 STAT5, such as epigenetic modifiers and transcriptional regulators, have been found throughout
403 the protein.[58] We used AI-assisted technology to generate tertiary structures of TERT and
404 STAT5 dimers and predict how they interact. AlphaFold[59] mapped the interaction between

405 human TERT and dimerized human STAT5a, and these binding data were visualized using
406 HDOCK[60] (**Supplemental Figure 5H and 5I**). Next, we tested TERT and STAT5 interaction by
407 expressing them exogenously. We fused the human CDS of TERT and STAT5 to NFAST and
408 CFAST splitFAST reporters, respectively, to generate TERT-NFAST and STAT5A-CFAST
409 fusion proteins. This approach allows monitoring of the formation and dissociation of a protein
410 assembly.[61] Control hVICs were co-transfected with TERT-NFAST and STAT5A-CFAST
411 plasmids and labeled with 5 µM HBR-3,5DOM (4-hydroxy-3,5- dimethoxy benzylidene
412 rhodamine) at d3, d5, and d7 of OST treatment or control NT. We found that the TERT/STAT5
413 splitFAST signal was highly elevated in calcifying control hVICs relative to the NT condition as
414 early as d3 throughout d7, supporting the early formation of the TERT/STAT5 complex in
415 calcifying hVICs (**Figure 4J**). Together, these approaches confirm TERT and STAT5 interaction
416 during osteogenic reprogramming.
417
418 To assess the function of TERT-STAT5 interaction, we performed chromatin
419 immunoprecipitation analysis (Ch-IP). We found that STAT5 is significantly enriched on both
420 putative STAT5 binding sites in the *RUNX2* promoter during osteogenic reprogramming (**Figure**
421 **4K**). *RUNX2* transcription is initiated from two distinct promoters: the distal promoter region P1,
422 located upstream of exon 1, and the proximal P2 promoter, located upstream of exon 2.[62,63] The
423 P1 promoter is highly active and required for osteoblast progenitor expansion, osteoblast
424 maturation, and bone formation, while the P2 promoter-derived isoform is expressed in
425 osteoblastic and non-osteoblastic mesenchymal cells.[64-66] Genome-wide CUT&Tag analysis of
426 the *Tert*$^{+/+}$ mVICs showed that STAT5 binds to the *Runx2* P1 and P2 promoters during
427 osteogenic differentiation and that STAT5 was absent in the same region of *Runx2* promoters in
428 *Tert*$^{-/-}$ mVICs, highlighting the Tert requirement for Stat5 binding to *Runx2* gene promoters
429 (**Figure 4L**, GEO accession GSE274226). Next, by comparing *Tert*$^{+/+}$ and *Tert*$^{-/-}$ CUT&Tag

430 sequencing of *Tert*$^{+/+}$ and *Tert*$^{-/-}$ mVICs, we found that Stat5 occupies promoter, intragenic, and
431 intergenic regions throughout the genome (**Figure 4M**). Gene Ontology (GO) pathway analysis
432 revealed that genes with high Stat5 binding participate in biological processes related to protein
433 phosphorylation, JAK/STAT signaling, inflammation, osteoblast differentiation, SMC function,
434 and chromatin remodeling (**Figure 4N**). Together, these data identify that TERT's effects are
435 mediated via STAT5 binding on the *Runx2* gene promoter and the promoters involved in several
436 pathways known to be operative during osteogenic reprogramming of cardiovascular cells.
437

438 **TERT and STAT5 are upregulated in calcified tissue.**

439 Confirming our in vitro and murine in vivo data above, in human CAVD tissue, we found that
440 STAT5 protein levels are significantly elevated and localized to areas of calcification in the
441 calcified leaflet, mirroring TERT distribution. Additionally, the number of STAT5-positive cells
442 was significantly higher in CAVD tissue compared to control tissue (**Figure 5A**). Furthermore,
443 the number of TERT/STAT5 co-positive nuclei was significantly greater in CAVD valves
444 compared to control valves (**Figure 5B**). These data support our in vitro investigations and
445 indicate that TERT/STAT5 interaction contributes to human CAVD pathogenesis.
446

447 **TERT interacts with SMARCA4 during the osteogenic reprogramming of VICs.**

448 Studies by others have shown that TERT facilitates chromatin accessibility and transcription by
449 recruiting SMARCA4 (previously referred to as BRG1), the catalytic subunit of the SWI/SNF
450 chromatin remodeling complex, to specific DNA loci.[18,67,68] We investigated whether SMARCA4
451 plays a role in the osteogenic reprogramming of hVICs via interacting with TERT. There was no
452 difference in SMARCA4 protein staining in the aorta of *Tert*$^{+/+}$ and *Tert*$^{-/-}$ mice fed the A6P6 diet,
453 nor in aortic rings ex vivo (**Supplemental Figures 6A and 6B**). However, in hVICs, expression
454 analysis revealed significant upregulation of *SMARCA4* transcripts as early as day five of OST

455 stimulation (**Supplementary Figure 6C**). Immunoprecipitation showed that TERT and
456 SMARCA4 physically interact in hVICs upon OST treatment (**Supplementary Figure 6D**).
457 Immunofluorescence staining showed that TERT and SMARCA4 are detected and colocalized
458 in cells in the calcified human leaflet (**Supplementary Figure 6E**), mirroring TERT and STAT5
459 distribution in human CAVD tissue. These findings suggest that SMARCA4 plays an active role
460 in the osteogenic reprogramming of VICs.
461

462 **DISCUSSION**

463 This study investigated the early steps required for the osteogenic reprogramming of human
464 valve interstitial cells in CAVD (**Figure 6**). This study establishes a critical role for TERT in this
465 process. Specifically, our data show that 1) TERT is upregulated in CAVD tissue and elevated in
466 primary VIC lines stimulated with osteogenic media. While TERT is elevated in these calcified
467 tissues and cells, telomere length is not impacted, nor is there evidence of cell senescence; 2)
468 TERT is required for the calcification of VICs, CASMCs, and MSCs. The requirement for TERT
469 occurs early in the process of osteogenic reprogramming, as knocking down TERT protein
470 levels after seven days of osteogenic stimulation did not deter calcification. These osteogenic
471 reprogramming activities of TERT are independent of its telomerase enzymatic activity, as *Terc*$^{-}$
472 $^{/-}$ cells or the use of the TERT enzymatic inhibitor BIBR1532 did not deter calcification.
473 Further, TERT co-immunoprecipitated with the chromatin remodeling enzyme SMARCA4, and
474 these two proteins were also found in the nucleus of CAVD tissues; 3) Inflammatory signals are
475 known to contribute to CAVD pathogenesis, and we found such signaling can increase TERT
476 levels, as well as the transcription factor STAT5. In silico modeling predicted TERT/STAT5
477 interaction, which was proven experimentally with immunoprecipitation, proximity ligation assay,
478 and a fluorescence complementation system developed for the visualization of transient protein-

479 protein interactions, and like TERT, genetic knockdown of STAT5, or specific inhibition of
480 STAT5 activity, prevented calcification. Lastly, the requirement for TERT was established in in
481 vivo and ex vivo calcification models. Collectively, these experiments support a novel role for
482 TERT and STAT5 in driving CAVD pathogenesis and cardiovascular reprogramming and
483 identify a unique, druggable target for cardiovascular calcification.
484
485 TERT is well-known for its canonical telomere-extending activity, yet TERT also regulates gene
486 expression and chromatin remodeling independent of affecting telomere integrity. TERT
487 interacts physically with several transcription factors to promote the expression of several
488 genes, including β-catenin, to stimulate genes involved in bone development.[15,16,49] In a wire-
489 injury restenosis model, TERT binds to the transcription factors SP1 at the *VEGF* promoter and
490 E2F1 at *MCM7*, *CCNA1*, and *PCNA* promoters, stimulating SMC proliferation and neointima
491 formation.[20,43,50,69] We did not detect proliferative or migratory differences between control and
492 CAVD VICs despite elevated levels of TERT at baseline (Figures 2B and 2C), indicating cell-
493 specific and stress-specific functions of TERT.
494
495 In addition to supporting transcription factor function, TERT can act as a cofactor to orchestrate
496 chromatin remodeling machinery. Studies have shown that TERT serves as a chaperone to
497 facilitate the recruitment of SMARCA4 and histone acetyltransferases to stimulate chromatin
498 accessibility and transcription or to maintain heterochromatin structure,[18,67,68] and loss of TERT
499 abrogates the cellular response to DNA double-strand breaks and alters the overall chromatin
500 configuration without affecting telomere integrity.[17] We now show that TERT is upregulated in
501 calcified valve tissues and VICs under osteogenic and inflammatory stimuli. TERT interacts with
502 STAT5, which binds to the *RUNX2* gene promoter and drives osteogenic reprogramming of the
503 aortic valve cells. TERT depletion reduced *RUNX2* expression and calcification in several cell

504 types, and TERT, STAT5, and the chromatin remodeling enzyme SMARCA4 co-
505 immunoprecipitated in OST-treated VICs (Supplementary Figure 6). Further, TERT and
506 SMARCA4 co-localized in the nucleus of CAVD tissues. These discoveries, along with the
507 findings of others showing that *TERT* overexpression drives osteogenic differentiation in human
508 MSCs,[21,22] support a broad role for TERT serving as a co-factor bridging chromatin remodeling
509 complexes and transcription factors to facilitate euchromatin formation to modulating cellular
510 phenotypic transition and osteogenic reprogramming.
511
512 Telomere length is considered a biomarker of aging, yet it varies widely between people of the
513 same age, even twins.[70] Several studies have utilized circulating leukocytes to investigate
514 whether shortened telomeres correlate with various vascular disease states.[71,72] One study
515 correlated telomere length in circulating leukocytes with aortic stenosis and found that leukocyte
516 telomere length was slightly shorter in individuals with aortic stenosis than in age-matched
517 controls.[73] However, telomere length in leukocytes does not indicate global telomere length in
518 an individual, telomerase complex activity, or TERT protein function in all cell types. Further,
519 somatic mosaicism and clonal hematopoiesis discoveries underscore the importance of not
520 ascribing telomere length in one cell type to telomere length and/or TERT activities in another.[74]
521 Short telomeres in circulating leukocytes may reflect increased cell turnover due to systemic
522 inflammation, as leukocytes are highly proliferative, and telomere attrition is highly likely to be a
523 tissue- and disease-dependent process. In this regard, Huzen et al. compared the telomere
524 length of the leukocytes of age-matched controls and patients with atherosclerosis and the
525 telomere length of the cells in the atherosclerotic plaques of the patients.[75] They found that
526 while telomere length in leukocytes from the atherosclerosis patient group was significantly
527 shorter than in the control group, telomere length in the atherosclerotic plaques was significantly
528 longer, indicative of increased telomerase activity. Thus, total leukocyte telomere length does

529 not represent telomere length in the diseased tissue. Our study investigated TERT protein levels
530 directly in the valve tissue and patient-specific VICs. We determined that the expression levels
531 of TERT and osteogenic markers in CAVD tissue and cells were elevated, without changes in
532 telomere length, proliferation, and DNA damage markers (Figures 1-2, Supplemental Figures 1-
533 4), suggesting non-canonical TERT activity in these cells.
534
535 VIC calcification shares aspects of the transcriptional program observed during the
536 differentiation of MSCs into osteoblasts, including the upregulation of *RUNX2, BGLAP, TNAP*,
537 and the secretion of bone-forming proteins and accumulation of calcium minerals.[10,12,76]
538 Likewise, signals such as mechanical stress, disturbed flow, and inflammation promote VIC
539 calcification and the osteogenic differentiation of MSCs.[77] These observations suggest that VICs
540 switch from their quiescent state and undergo an osteogenic reprogramming akin to the
541 differentiation of MSCs into osteoblasts, acquiring a calcifying phenotype. The mechanisms
542 coordinating the early molecular events in these cell transitions have yet to be fully understood.
543 We have hypothesized that fully differentiated cells can de-differentiate into a transitory,
544 multipotent stem cell-like state and then acquire an osteogenic phenotype.[78] VICs exhibit the
545 potential to differentiate into osteogenic, chondrogenic, or adipogenic lineages, properties
546 comparable to mesenchymal stem cells.[79] We chose to investigate TERT in the osteogenic
547 reprogramming of VICs as TERT is highly expressed in stem cells, and its overexpression
548 primes mesenchymal stem cells into the osteogenic lineage.[21,22] Our data supports the role of
549 TERT in the osteogenic reprogramming of VICs, whereby TERT serves as a bridge between
550 DNA-binding transcription factors and chromatin remodeling enzymes.
551
552 The osteogenic differentiation of stem cells is orchestrated by RUNX2, which is also detected in
553 the osteogenic reprogramming of valvular and vascular cells.[32,33] In a recent transcriptomic

554 study, Xu et al. identified 14 cell populations in aortic valve tissue samples from two control and
555 four CAVD valves.[80] The severity of CAVD was assessed via ultrasound imaging, which detects
556 leaflet mobility; however, examining the macroscopic pictures and histological staining of valve
557 leaflets used in this analysis shows that while these valves are indeed stiff, they do not exhibit
558 robust nodules of calcification as do the valves in our data set (Figures 1A, 1C, 5, and
559 Supplemental Figure 1A). Their analysis identified three VIC populations defined by expression
560 of *FOS, HSPA6, and SPARC.* However, cells from six valves were pooled, with 10.4% of cells
561 from control tissue and the remaining 89.6% from CAVD tissues. Bulk transcriptomic data from
562 these tissues show only a small 1.49-fold increase in *RUNX2* gene expression in CAVD tissues,
563 in stark contrast with our more stringent analysis of *RUNX2* expression by quantitative PCR
564 (Figure 2, Supplemental Figure 4) and what is currently accepted.[10-12] Inspection of the publicly
565 available bulk RNA-sequencing data (PRJNA552159) showed no increase in *TERT* transcript
566 expression. While the hemodynamic data showed those valves had undergone fibrotic
567 remodeling, few calcifying cells were present, as seen by their histological staining. This lack of
568 calcification may explain why TERT expression was undetected in their study. In the general
569 population, aortic sclerosis commonly goes undetected until a patient develops symptoms such
570 as dyspnea, angina, and syncope, as the stiffness and remodeling of the leaflet obstructs
571 ventricular outflow. A population-based study assessed aortic valve disease in 552 randomly
572 selected men and women aged 55 to 86. Using imaging and Doppler echocardiography, mild
573 calcification was observed in 40% of the individuals, severe calcification in 13%, and
574 symptomatic stenosis in only 2.2%.[81] This population-based study illustrates how common aortic
575 valve remodeling is and highlights the importance of using multiple modalities to accurately
576 determine valve pathology (i.e., fibrotic vs calcified). In our study, a portion of each patient valve
577 was used for cell isolation while the rest was utilized for calcification assessment by histological
578 staining, following a workflow that we developed that guarantees that cells isolated from

579 surgically removed and postmortem tissues retain their proliferative capacity and endothelial
580 and interstitial phenotypes in culture.[29] While unbiased sequencing approaches can help
581 uncover novel mechanisms contributing to disease states, they are skewed towards expression
582 in a snapshot and can miss short-lived transitory events.
583
584 The function of STAT5 in bone formation is multifaceted. While it was shown that STAT5 could
585 promote the differentiation of MSCs into osteoblasts by upregulating the osteogenic genes in a
586 Jak2-dependent manner, a Stat5a global knockout mouse exhibited elevated bone mass and
587 mineral density.[82,83] These conflicting reports indicate that the role of STAT5 in bone formation
588 and remodeling is complex, and more studies are required. STAT5 has diverse functions as a
589 transcription factor: it interacts with histone acetyltransferases and transcription factors such as
590 the glucocorticoid receptor, SP1, YY1, and C/EBPβ to stimulate gene expression,[84-86] and
591 studies in cancer cells identified that STAT5 can induce *TERT* expression.[87,88] In silico modeling
592 found multiple putative STAT5 binding sites in the *RUNX2* P1 promoter region, which were
593 confirmed with Ch-IP assays. This confirms that STAT5/TERT acts to initiate the osteogenic
594 reprogramming of VICS, establishing a novel mechanism in CAVD pathogenesis whereby
595 TERT/STAT5 bind to each other and activate osteogenic gene transcription, which drives the
596 early events in cellular osteogenic reprogramming. Cell phenotype reprogramming requires
597 chromatin restructuring to allow for the transcription of repressed genes. As observed in other
598 cell types, we found TERT co-immunoprecipitated with SMARCA4, as well as STAT5, and
599 genetic depletion of TERT or STAT5 midway through the OST assay (i.e., day 14) did not
600 perturb the calcification of cells. This observation strongly supports that TERT complexes with
601 SMARCA4 to remodel chromatin and with the STAT5 transcription factor to bind and activate
602 *RUNX2* gene transcription. We explored the potential physical direct interaction between TERT
603 and STAT5, and we propose that the RNA binding domain of TERT is the most likely candidate

604 to interact with STAT5 (Supplemental Figure 5). Studies identifying critical domains for
605 interaction are currently ongoing.
606
607 The strengths of this study lie in the utilization of human and mouse tissues and primary lines
608 generated from valve leaflets. While our results are robust, it is important to address the
609 limitations of our study. Firstly, we worked with a limited number of human samples obtained
610 from cadaveric donors who matched sex and age. Due to this limited sample size, we limited
611 our statistical analyses to non-parametric analysis, comparing two to four groups, and no mixed
612 models were included. Regardless, one strength of our study is the multiprong approach to
613 determining the role of TERT and STAT5 in vascular calcification. Secondly, STAT5A and
614 STAT5B are two different genes, with 96% of their amino acid sequence shared and their
615 activities redundant.[25] We have determined that VICs express both variants; however, our
616 antibodies and shRNA constructs could not differentiate between the two variants. Thus, the two
617 isoforms may interact with TERT to bind the *RUNX2* gene promoter. STAT5 is activated by
618 multiple cytokines, including IL-2, IL-6, and TNF-α, and it was shown that IL-2 specifically
619 activates STAT5 to induce TERT expression in cancer cells.[87,89] Whether STAT5 first induces
620 TERT expression and then TERT and STAT5 cooperate to control the expression of *RUNX2*
621 needs to be determined. Thirdly, there is redundancy regarding STAT1/3/5 functions and
622 signaling.[90] Our study was not designed to address all the complexities of STAT signaling per se
623 but rather to investigate the role of TERT as a key protein that orchestrates the osteogenic
624 reprogramming of aortic valve cells; our future studies will explore the role of STAT5 further.
625
626 Our work highlights the importance of primary human tissue-based studies. Murine models are
627 not ideal for studying non-genetic drivers of CAVD, as mice do not develop CAVD de novo.[91,92]
628 Mouse leaflets' structure differs from human leaflets as they lack a trilaminar organization and

629 present a melanocyte cell population.[93-95] Recent elegant work from the Giachelli group showed
630 that in mice, calcification happens in the sinus wall and, to a lesser extent, at the leaflet hinge,
631 the region between the leaflet VICs and SMCs of the aorta, with no detectable calcification in
632 the aortic valve leaflets after 26 weeks of a high-fat diet in a *Ldlr* knockout mice model.[96] This
633 distribution of aortic root calcification is also observed in a mouse model described by a Honda
634 et al which detected calcification in the sinus wall 16 weeks post wire-induced mechanical
635 injury.[91] Due to the lack of aortic valve leaflet calcification in atherosclerotic or mechanical injury
636 murine models, we utilized a diet-induced medial arterial calcification (MAC) model.[45] MAC is
637 not associated with lipid deposition, fibrous cap formation, or intimal hyperplasia; instead, MAC
638 stems from the progressive accumulation of calcium and phosphate within the arterial walls.[97]
639 These structural features distinguish MAC from atherosclerosis and are more representative of
640 the pathogenesis of valve leaflet calcification.[2,97]
641
642 This study has uncovered the early molecular events that enable the osteogenic reprogramming
643 of the interstitial cells of the aortic valve. Current CAVD therapies are surgical, limited to
644 mechanical or bioprosthetic valve replacement, and performed only when the disease has
645 progressed to the advanced point of affecting blood flow and heart function. Our data show that
646 perturbing TERT or STAT5 can inhibit calcification; however, broadly inhibiting one or the other
647 of these proteins may have deleterious off-target effects. Understanding the specific binding
648 domains and other protein binding partners of TERT and STAT5 will enable the development of
649 small molecules to block their interaction, which is a more feasible therapeutic strategy for aortic
650 valve calcification than global inhibition. CAVD affects over 9.5 million people in the U.S. and
651 has an associated 56-67% 5-year mortality rate; hence, the need for early, non-surgical
652 therapies is great.[4] This study uncovers a novel and targetable pathway that may be leveraged
653 to halt or prevent CAVD progression.

654

655 **ACKNOWLEDGEMENTS**

656 We want to acknowledge and thank the Center for Organ Research and Education for their help
657 and support, as well as tissue donors and their families for making this study possible. We thank
658 Dr. Alison Tebo for her guidance and assistance in constructing the SplitFAST plasmids tool
659 used in this study. We would also like to thank Kristin Konopka, tissue bank coordinator at The
660 Department of Cardiothoracic Surgery, UPMC. We thank Jason Dobbins for his critical reading
661 of this manuscript.

662

663 **SOURCES OF FUNDING**

664 This study was supported by funds from the National Institutes of Health (R01 HL142932, R56
665 HL168657, St. Hilaire), the American Heart Association (20IPA35260111, St. Hilaire; 902641,
666 Cuevas; 24POST1186619, Behzadi), the McKamish Family Foundation (St. Hilaire and Sultan)
667 and the Samuel and Emma Winters Foundation (St. Hilaire).

668

669 **DISCLOSURES**

670 The University of Pittsburgh has filed a provisional patent application regarding technology on
671 behalf of CSH and RAC based on the findings presented in this manuscript. IS receives
672 institutional research support from Atricure and Medtronic and is a consultant for Medtronic
673 Vascular. None of these conflicts of interest are related to this work. All other authors have nothing
674 to disclose.

675

676 **FIGURE LEGENDS**

677 **Figure 1. TERT is elevated in CAVD tissues.** (A) Examples of non-calcified control (top) and
678 calcified CAVD (bottom) human valves used in this study. Arrowheads indicate calcified nodules

679 Scalebar. 1 cm. (B), TERT mRNA transcript quantification in control and CAVD valve tissues. n
680 = 8 control, n= 9 CAVD. (C), Representative serial sections of Von Kossa (dark precipitation)
681 and TERT immunofluorescent staining in control and CAVD valve tissues. Scalebar 100 µm.
682 Graphs show the quantification of TERT intensity and the number of TERT-positive cells. n = 9
683 control, n = 9 CAVD. (D), Telomere length measurements in valve tissues. n = 19 control, n =
684 12 CAVD. (E), Age of the patients utilized in this study. n = 25 control, n = 16 CAVD. Data are
685 shown as means ± SD. P values were calculated using the Mann-Whitney U test and shown on
686 each graph. L = lumen.
687
688 **Figure 2. TERT is elevated in CAVD hVICs at baseline and upregulation during**
689 **osteogenic reprogramming.** (A), Representative images showing cell morphology of control
690 and CAVD hVICs. Scalebar 50 µm. (B), Proliferation of control and CAVD hVICs at baseline. n
691 = 3 both groups. (C) Relative migration distances of control and CAVD VICs. n = 10 both
692 groups. (D) Western blot staining of control and CAVD hVICs at baseline. Quantification of
693 protein levels is shown on the right panels. n = 4 both groups. (E) Telomere length
694 measurements in VICs. n = 8, control, n = 5 CAVD. (F) Representative images of early
695 calcification in hVICs growing in normal conditions (no treatment NT) or stimulated with
696 osteogenic media (OST) for 14 days. Calcium deposition was visualized by Alizarin Red
697 staining. Scalebar 50 µm. Quantification of calcification on the right graphs. n = 7 both groups.
698 (G), Western blot staining of samples from control and CAVD hVICs after 14 days of NT or
699 OST. Quantification of protein levels is shown on the bottom graphs. n = 4 both groups. (H),
700 Representative immunofluorescent staining images of TERT in control and CAVD hVICs after
701 14 days of NT or OST. Calcium deposition was visualized with OsteoImage. Scalebar 100 µm.
702 (I) Expression profile control VICs after 14 days of NT and OST treatment. n = 4 both groups.
703 Data are shown as means ± SD. P values were calculated by 2-way ANOVA (Figure C), the

704 Mann-Whitney U test (Figures B, D, E, G, and I), and the Kruskal-Wallis H test with Dunn post
705 hoc test Figure F) and shown on each graph. * P = 0.0286 in Figure I.
706
707 **Figure 3. TERT is required to initiate osteogenic transition and calcification.** (A) Control
708 hVICs were transduced lentivirus containing shControl or shTERT and followed by OST
709 stimulation for up to 28 days. Calcium deposition was visualized by Alizarin Red staining. n = 6
710 shControl, n = 6 shTERT at 21 days and n = 9 each group at day 28. Scalebar 400 µm. (B)
711 Representative western blot staining of control hVICs transduced with lentivirus containing
712 either shControl or shTERT followed by 7 days of OST. (C) hCASMCs were transduced with
713 shControl or shTERT and stimulated with OST for 14 and 21 days. n = 4 for each group at both
714 time points. Scalebar 400 µm. (D) Representative images of mVIC isolated from *Tert*$^{+/+}$ and *Tert*
715 $^{-/-}$ mice were stimulated with OST for 28 days. Scalebar 400 µm. (E) Representative Von Kossa
716 staining images of *Tert*$^{+/+}$ and *Tert*$^{-/-}$ mice aortas (dark precipitation). Scale bar 400 µm.
717 Quantification of calcification is shown on the right panel. (F) Representative immunofluorescent
718 images of Runx2 expression indicative of calcification (red, insert) on *Tert*$^{+/+}$ and *Tert*$^{-/-}$ mice
719 aorta. Scale bar 400 *µ*m. Runx2 quantification of calcification is shown on the right panel. (G)
720 Representative images of mVICs isolated from F1 *Tert*$^{-/-}$ *or Terc*$^{-/-}$ mice were stimulated with
721 OST for up to 21 days. Scalebar 100 µm. Data are shown as means ± SD. P values were
722 calculated using the Kruskal-Wallis H test, Dunn post hoc test (Figures A, C, and G), and Mann-
723 Whitney U test (Figures D, E, and F).
724
725 **Figure 4. STAT5 binds to TERT and is required for the calcification of human VICs.** (A)
726 Graphic of in silico analysis identifying the consensus binding site for STAT5. (B), Diagram
727 depicting STAT5 binding to RUNX2 promoter and the positions of the predicted STAT5 binding
728 sites (purple boxes). (C) Representative immunofluorescence images of control hVICs after 14

729 days of LPS treatment or OST stimulation. Scalebar 50 µm. (D) Representative western blot
730 staining of hVICs after 14 days of OST stimulation. (E) Representative images of control hVICs
731 treated with 10 µM of the STAT5 inhibitors StafiA-1 or StafiB-1 throughout 28 days of
732 osteogenic stimulation. Scalebar 400 µm. n = 8 each group. The quantification of calcification is
733 shown on the right graph. (F) Control hVICs were transduced with lentivirus containing
734 shControl or shSTAT5 constructs and treated with OST for 21 days. Calcium deposition was
735 visualized by Alizarin Red staining. n = 9 for each group. Scalebar 400 µm. (G) Representative
736 images of hVIC (left panels) treated with 10 µM of the STAT5 inhibitors StafiA-1 starting at d7 or
737 d14 of OST treatment. Samples were collected at d21. Scalebar 400 µm. n = 6 for each group.
738 (H) Representative images of TERT/STAT5 complex (red foci) in control hVICs cultured for 21
739 days in osteogenic medium and detected by PLA. Scalebar 100 µm. n = 4 for each group. (I)
740 TERT/STAT5 interaction was detected by co-immunoprecipitation in control hVICs under OST
741 for 21 days. (J) Control hVIC co-expressing TERT-NFAST and STAT5A-CFAST were labeled
742 with 5 µM HBR-3,5DOM (4-hydroxy-3,5- dimethoxybenzylidene rhodamine, coral) and imaged
743 at d3, d5, and d7 of osteogenic treatment (OST) or control no-treatment (NT). Scale bars 50
744 µm. (K) Chromatin immunoprecipitation shows enrichment of STAT5 on RUNX2 promoter OST
745 conditions compared to NT. The base position is indicated in the blue boxes. n=4 for each group
746 as in B. (L) STAT5 CUT&Tag sequencing tracks in genomic regions of Runx2 in no-treatment
747 control and osteogenic condition-treated mice VICs. (M) Stacked chart representing genome-
748 wide STAT5 occupancy in promoters, genes, and intergenic regions frequency in mice VICs. (N)
749 Top 20 GO pathways enriched in genes with significant loss of STAT5 in *Tert*$^{+/+}$vs *Tert*$^{-/-}$ mice
750 VICs. Data are shown as means ± SD. P values were calculated by the Mann-Whitney U test
751 (Figures F, H, and J) and the Kruskal-Wallis H test (Figures E and G) and indicated on top of
752 each graph.
753

754 **Figure 5. TERT and STAT5 are upregulated and colocalized in CAVD tissue.** (A)
755 Representative serial sections of Von Kossa (dark precipitation) and TERT and STAT5
756 immunofluorescent staining in control and CAVD tissues. Scalebar 100 µm. STAT5 intensity
757 and STAT5-positive cells (STAT5+) are quantified on the right panels. (B) Quantification of
758 STAT5-TERT-positive cells. Data are shown as means ± SD, n = 5 control, n = 6 CAVD. P
759 values were calculated with the Mann-Whitney U test and indicated on each graph. L = lumen.
760

761 **Figure 6. TERT/STAT5 promotes osteogenic reprogramming.** Inflammatory signals promote
762 the upregulation and interaction of TERT and STAT5A. The TERT/STAT5 complex translocates
763 into the nucleus, where TERT interacts with SMARCA4 (also known as BRG1), which facilitates
764 a permissive chromatin configuration, and STAT5A binds specific sites on the RUNX2 promoter,
765 leading to the osteogenic reprogramming of valve interstitial cells during the early stages of
766 CAVD pathogenesis.
767

768 **Supplemental Figure 1. Characterization of human CAVD valves and patient-isolated**
769 **VICs at baseline.** (A) Representative section of Von Kossa staining in control and valve CAVD
770 leaflets tissue. Scalebar 1 mm. (B) Representative serial sections of RUNX2 immunofluorescent
771 staining and OPN in control and CAVD valve tissues. Scalebar 100 µm. Quantification of
772 RUNX2-positive cells and OPN-positive cells on the leaflet specimen is shown on the right
773 graphs. n = 5 control, n = 6 CAVD. (C) Correlation between age of the donor and TERT
774 expression in valve tissues. n = 8 control, n = 9 CAVD. (D) Gene expression profile in the valve
775 leaflets. n = 7 each group. (E) Representative images of immunofluorescent staining of PCNA
776 (top panels) and γ-H2AX (bottom panels) in control and CAVD valve tissues. Scalebar 100 µm.
777 Quantification of PCNA-positive cells and γ-H2AX-positive cells are shown on the right graphs.
778 n = 4 control, n = 3 CAVD. (F) Representative images of a scratch assay in control and CAVD

779 hVICs. Time points are indicated on top of each panel. Blue lines denote the cell migration front.
780 Scalebar 1 mm. n = 10 of each group. (G) Representative images of αSMA, CNN, SM22, TNAP,
781 and f-Actin in control and CAVD hVICs. Scalebar 50 µm. Signal quantification is shown on the
782 right. n = 4 each group. Data are shown as means ± SD. P values were calculated with the
783 Mann-Whitney U test (Figures A, B, D, F, and G), Pearson correlation test (Figure C), and two-
784 way ANOVA with the Sidak post hoc test (Figure D and shown on top of each graph). L =
785 lumen.
786
787 **Supplemental Figure 2. Inhibition of reverse transcriptase activity of TERT does not**
788 **prevent osteogenic reprogramming of hVICs.** (A) Cell counts of control and CAVD hVICs
789 after 14 days of NT or OST stimulation. n = 4 each group. (B) β-galactosidase (BLG1) mRNA
790 transcript quantification in control and CAVD hVICs at baseline. n = 5 control, n= 4 CAVD. (C)
791 Representative images of senescence-associated β-galactosidase activity staining of hVICs
792 after 28 days of NT or OST stimulation. Blue cells were considered positive for senescence.
793 Quantification of senescence is shown on the right graph. n = 4 each group. Data are shown as
794 means ± SD. P values were calculated with the Mann-Whitney U test (Figure B) and the
795 Kruskal-Wallis H test with Dunn pairwise comparison post hoc test (Figures A, C) and shown on
796 top of each graph. Scalebar 400 µm. n = 6 for each group.
797
798 **Supplemental Figure 3. TERT is upregulated and required for the osteogenic**
799 **differentiation of human mesenchymal stem cells**. (A) Representative images of hMSCs
800 stimulated with OST for 14 days. Calcium deposition was visualized by Alizarin Red staining.
801 Scalebar 50 µm. (B) Western blot staining of samples from hMSCs collected during the 14 days
802 of OST treatment. (C) RUNX2 expression profile of differentiating hMSCs stimulated for 14 days
803 with OST media. n = 3. (D) Representative TERT immunofluorescent staining images of hMSCs

804 stimulated with OST for 14 days. Scalebar 100 µm. (E) Representative images of hMSCs
805 infected with shTERT or shControl virus and stimulated with OST for 14 days. Calcium
806 deposition was visualized by Alizarin Red staining. The quantification of calcification is shown
807 on the right graph. n = 3. (F) Western blot staining of samples from hMSCs collected during the
808 14 days of OST treatment. Data are shown as means ± SD. P values were calculated with the
809 Kruskal-Wallis H test with Dunn pairwise comparison post hoc test (Figure C) and the Mann-
810 Whitney U test (Figure E) and shown on each graph.
811
812 **Supplemental Figure 4. Inhibition of reverse transcriptase activity of TERT does not**
813 **prevent osteogenic reprogramming of VICs.** (A) Representative images of mBMMSCs
814 isolated from *Tert*$^{+/+}$ or *Tert*$^{-/-}$ mice and stimulated with OST for 21 days. Scalebar 100 µm.
815 Quantification of calcification is presented as average absorbance on the right graphs, n = 5 for
816 each group. (B, C) Representative images of a senescence-associated β-galactosidase (SA-β-
817 gal) staining of mVICs and mBMMSCs isolated from *Tert*$^{+/+}$ or F1 *Tert*$^{-/-}$ mice after 21 days of
818 OST stimulation. In each group, blue cells were considered positive for senescence, n = 5. (D)
819 Schematic of OST treatment with delayed shTERT transduction (top panel). VICs were
820 transduced with shTERT, and calcification was assessed with Alizarin Red S stain at day 21.
821 Scalebar 400 µm. n = 6 for each group. (E) Representative sections of Von Kossa staining in
822 thoracic aortic rings isolated from *Tert*$^{+/+}$ and *Tert*$^{-/-}$ mice after 14 days of OST treatment relative
823 to NT control treatment. Quantification is shown on the right. Scale bar 400 μm (F)
824 Immunofluorescence staining of thoracic aortic rings after OST treatment as in B. Quantification
825 of Runx2 is shown on the right graph. Scale bar 400 μm (G) Western blot staining of aortic ring
826 specimens collected and treated in B. Quantification of Runx2 is shown on the right graph. (H)
827 Human VICs were treated with the TERT inhibitor BiBR1532 and stimulated with OST, and
828 calcification was assessed on day 28, with n = 5 in each group. (I) TERT, RUNX2, and STAT5A

829 expression were evaluated on day 14, n = 6 DMSO, n = 5 BIBR1532. Data are shown as means
830 ± SD. P values were calculated with the Kruskal-Wallis H test with Dunn pairwise comparison
831 post hoc test (Figures A, B, C, E, H) and the Mann-Whitney U test (Figures D, F, G, I) and are
832 shown on top of each graph.
833
834 **Supplemental Figure 5. STAT5 is upregulated, binds to TERT, and is required for**
835 **osteogenic reprogramming of VICs.** (A) Western blot analysis of cytoplasmic and nuclear
836 fractions of TERT from control VICs obtained after seven days of OST stimulation. Fractions
837 purity was assessed by staining for markers of cytoplasm (TUB) and nucleoplasm (Histone H3).
838 Cyt, cytoplasmic fraction; Nuc, nuclear fraction. (B) Representative immunofluorescence image
839 of STAT5 shows subcellular distribution after 14 days of NT and OST stimulation. Scalebar 40
840 µm. (C) Representative images of CASMCs treated with 10 µM of the STAT5 inhibitors StafiA-1
841 or StafiB-1 during the 14 days of OST stimulation. Scalebar 400 µm. n = 4 for each group. (D)
842 Representative images of MSCs treated with 10 µM of the STAT5 inhibitors StafiA-1 or StafiB-1
843 during the 21 days of OST stimulation. Scalebar 400 µm. n = 4 for each group. (E)
844 Representative images of TERT/STAT5 complex (red foci) detected by proximity ligation assay
845 (PLA) in the nucleus of control VICs. Scalebar 25 µm. The PLA foci quantification and intensity
846 are shown on the right graph. n = 4 for each group. (H) Mol*3D Viewer rendering of the TERT-
847 STAT5 dimer interaction predicted by the HDock. Red boxes indicate the position of the
848 interaction between TERT and STAT5. (F) Representative immunofluorescent images of Stat5
849 expression after 12 weeks of high adenine high phosphate diet on *Tert*$^{-/-}$ and *Tert*$^{-/-}$ mice aorta.
850 Scale bar 400 μm. Quantification of Stat5 expression is shown on the right panel. (G)
851 Representative images of Stat5 immunofluorescence staining of thoracic aortic rings isolated
852 from *Tert*$^{+/+}$ and *Tert*$^{-/-}$ mice after 14 days of OST treatment relative to NT control treatment.
853 Quantification of Stat5 is shown on the right graph. Scale bar 400 μm (I) The diagram shows the

854 regions involved in the predicted interaction as indicated in A, and the docking and confidence
855 scores predicted by HDock are indicated. TEN: DNA anchor domain for processive telomeric
856 repeat addition, RBD: Telomerase RNA binding domain, RT: Finger and palm region of the
857 reverse transcriptase domain, CTE: C-terminal extension or putative thumb domain of the
858 reverse transcriptase, CCD: Coiled-coil domain, required for nuclear localization, DBD: DNA
859 binding domain, HLK: Helical linker and DNA binding domain, SH2: Domain required for
860 activation and dimerization, TD: Transactivation domain. Data are shown as means ± SD. P
861 values were calculated with the Mann-Whitney U test (Figures A and G) and the Kruskal-Wallis
862 H test with Dunn pairwise comparison post-test (Figures B, E, and F) and indicated in each
863 graph.
864
865 **Supplemental Figure 6. Chromatin remodeling enzyme SMARCA4 is upregulated and**
866 **interacts with TERT during the osteogenic reprogramming of VICs.** (A) Representative
867 immunofluorescent images of Smarca4 expression after 12 weeks of high adenine high
868 phosphate diet on *Tert*$^{-/-}$ and *Tert*$^{-/-}$ mice aorta. Scale bar 400 μm. Quantification of Smarca4
869 expression is shown on the right panel. (B) Representative images of Smarca4
870 immunofluorescence staining of thoracic aortic rings isolated from *Tert*$^{+/+}$ and *Tert*$^{-/-}$ mice after
871 14 days of OST treatment relative to NT control treatment. Quantification of Smarca4 is shown
872 on the right graph. (C) SMARCA4 expression was evaluated on days 5 and 10 on VICs
873 stimulated with OST. n = 5 each group. (E) TERT/STAT and TERT/SMARCA4 interaction was
874 detected by co-immunoprecipitation upon osteogenic stimulation on VIC. (E) Representative
875 TERT and SMARCA4 immunofluorescent staining in control and CAVD tissues. The number of
876 positive cells is shown on the right graphs. n = 9 control, n = 9 CAVD. Scalebar 100 µm. Data
877 are shown as means ± SD, and P values were calculated with the Mann-Whitney U test and
878 indicated on each graph in Figures A and C. L = lumen.

879

880 **REFERENCES**

881 1. Kraler S, Blaser MC, Aikawa E, Camici GG, Luscher TF. Calcific aortic valve disease:
882 from molecular and cellular mechanisms to medical therapy. *Eur Heart J*. 2022;43:683-
883 697. doi: 10.1093/eurheartj/ehab757
884 2. Small AM, Yutzey KE, Binstadt BA, Voigts Key K, Bouatia-Naji N, Milan D, Aikawa E,
885 Otto CM, St Hilaire C, American Heart Association Council on G, et al. Unraveling the
886 Mechanisms of Valvular Heart Disease to Identify Medical Therapy Targets: A Scientific
887 Statement From the American Heart Association. *Circulation*. 2024;150:e109-e128. doi:
888 10.1161/CIR.0000000000001254
889 3. Buttner P, Feistner L, Lurz P, Thiele H, Hutcheson JD, Schlotter F. Dissecting Calcific
890 Aortic Valve Disease-The Role, Etiology, and Drivers of Valvular Fibrosis. *Front*
891 *Cardiovasc Med*. 2021;8:660797. doi: 10.3389/fcvm.2021.660797
892 4. Coffey S, Roberts-Thomson R, Brown A, Carapetis J, Chen M, Enriquez-Sarano M,
893 Zuhlke L, Prendergast BD. Global epidemiology of valvular heart disease. *Nat Rev*
894 *Cardiol*. 2021;18:853-864. doi: 10.1038/s41569-021-00570-z
895 5. Roth GA, Mensah GA, Johnson CO, Addolorato G, Ammirati E, Baddour LM, Barengo
896 NC, Beaton AZ, Benjamin EJ, Benziger CP, et al. Global Burden of Cardiovascular
897 Diseases and Risk Factors, 1990-2019: Update From the GBD 2019 Study. *J Am Coll*
898 *Cardiol*. 2020;76:2982-3021. doi: 10.1016/j.jacc.2020.11.010
899 6. Virani SS, Alonso A, Benjamin EJ, Bittencourt MS, Callaway CW, Carson AP,
900 Chamberlain AM, Chang AR, Cheng S, Delling FN, et al. Heart Disease and Stroke
901 Statistics-2020 Update: A Report From the American Heart Association. *Circulation*.
902 2020;141:e139-e596. doi: 10.1161/CIR.0000000000000757
903 7. Rajamannan NM, Evans FJ, Aikawa E, Grande-Allen KJ, Demer LL, Heistad DD,
904 Simmons CA, Masters KS, Mathieu P, O'Brien KD, et al. Calcific aortic valve disease:
905 not simply a degenerative process: A review and agenda for research from the National
906 Heart and Lung and Blood Institute Aortic Stenosis Working Group. Executive summary:
907 Calcific aortic valve disease-2011 update. *Circulation*. 2011;124:1783-1791. doi:
908 10.1161/CIRCULATIONAHA.110.006767

909 8. Chen JH, Simmons CA. Cell-matrix interactions in the pathobiology of calcific aortic
910 valve disease: critical roles for matricellular, matricrine, and matrix mechanics cues. *Circ*
911 *Res*. 2011;108:1510-1524. doi: 10.1161/CIRCRESAHA.110.234237
912 9. Liu AC, Joag VR, Gotlieb AI. The emerging role of valve interstitial cell phenotypes in
913 regulating heart valve pathobiology. *Am J Pathol*. 2007;171:1407-1418. doi:
914 10.2353/ajpath.2007.070251
915 10. Rajamannan NM, Subramaniam M, Rickard D, Stock SR, Donovan J, Springett M,
916 Orszulak T, Fullerton DA, Tajik AJ, Bonow RO, et al. Human aortic valve calcification is
917 associated with an osteoblast phenotype. *Circulation*. 2003;107:2181-2184. doi:
918 10.1161/01.CIR.0000070591.21548.69
919 11. Rajamannan NM. Calcific aortic valve disease: cellular origins of valve calcification.
920 *Arterioscler Thromb Vasc Biol*. 2011;31:2777-2778. doi: 10.1161/ATVBAHA.111.237610
921 12. Aikawa E, Libby P. A Rock and a Hard Place: Chiseling Away at the Multiple
922 Mechanisms of Aortic Stenosis. *Circulation*. 2017;135:1951-1955. doi:
923 10.1161/CIRCULATIONAHA.117.027776
924 13. Wirrig EE, Yutzey KE. Conserved transcriptional regulatory mechanisms in aortic valve
925 development and disease. *Arterioscler Thromb Vasc Biol*. 2014;34:737-741. doi:
926 10.1161/ATVBAHA.113.302071
927 14. Calado RT, Young NS. Telomere diseases. *N Engl J Med*. 2009;361:2353-2365. doi:
928 10.1056/NEJMra0903373
929 15. Stewart SA, Hahn WC, O'Connor BF, Banner EN, Lundberg AS, Modha P, Mizuno H,
930 Brooks MW, Fleming M, Zimonjic DB, et al. Telomerase contributes to tumorigenesis by
931 a telomere length-independent mechanism. *Proc Natl Acad Sci U S A*. 2002;99:12606-
932 12611. doi: 10.1073/pnas.182407599
933 16. Choi J, Southworth LK, Sarin KY, Venteicher AS, Ma W, Chang W, Cheung P, Jun S,
934 Artandi MK, Shah N, et al. TERT promotes epithelial proliferation through transcriptional
935 control of a Myc- and Wnt-related developmental program. *PLoS Genet*. 2008;4:e10.
936 doi: 10.1371/journal.pgen.0040010
937 17. Masutomi K, Possemato R, Wong JM, Currier JL, Tothova Z, Manola JB, Ganesan S,
938 Lansdorp PM, Collins K, Hahn WC. The telomerase reverse transcriptase regulates
939 chromatin state and DNA damage responses. *Proc Natl Acad Sci U S A*.
940 2005;102:8222-8227. doi: 10.1073/pnas.0503095102

941 18. Park JI, Venteicher AS, Hong JY, Choi J, Jun S, Shkreli M, Chang W, Meng Z, Cheung
942 P, Ji H, et al. Telomerase modulates Wnt signalling by association with target gene
943 chromatin. *Nature*. 2009;460:66-72. doi: 10.1038/nature08137
944 19. Aono J, Ruiz-Rodriguez E, Qing H, Findeisen HM, Jones KL, Heywood EB, Bruemmer
945 D. Telomerase Inhibition by Everolimus Suppresses Smooth Muscle Cell Proliferation
946 and Neointima Formation Through Epigenetic Gene Silencing. *JACC Basic Transl Sci*.
947 2016;1:49-60. doi: 10.1016/j.jacbts.2016.01.002
948 20. Endorf EB, Qing H, Aono J, Terami N, Doyon G, Hyzny E, Jones KL, Findeisen HM,
949 Bruemmer D. Telomerase Reverse Transcriptase Deficiency Prevents Neointima
950 Formation Through Chromatin Silencing of E2F1 Target Genes. *Arterioscler Thromb*
951 *Vasc Biol*. 2017;37:301-311. doi: 10.1161/ATVBAHA.116.308717
952 21. Shi S, Gronthos S, Chen S, Reddi A, Counter CM, Robey PG, Wang CY. Bone
953 formation by human postnatal bone marrow stromal stem cells is enhanced by
954 telomerase expression. *Nat Biotechnol*. 2002;20:587-591. doi: 10.1038/nbt0602-587
955 22. Simonsen JL, Rosada C, Serakinci N, Justesen J, Stenderup K, Rattan SI, Jensen TG,
956 Kassem M. Telomerase expression extends the proliferative life-span and maintains the
957 osteogenic potential of human bone marrow stromal cells. *Nat Biotechnol*. 2002;20:592-
958 596. doi: 10.1038/nbt0602-592
959 23. Leonard WJ, O'Shea JJ. Jaks and STATs: biological implications. *Annu Rev Immunol*.
960 1998;16:293-322. doi: 10.1146/annurev.immunol.16.1.293
961 24. Hu X, Li J, Fu M, Zhao X, Wang W. The JAK/STAT signaling pathway: from bench to
962 clinic. *Signal Transduct Target Ther*. 2021;6:402. doi: 10.1038/s41392-021-00791-1
963 25. Okutani Y, Kitanaka A, Tanaka T, Kamano H, Ohnishi H, Kubota Y, Ishida T, Takahara
964 J. Src directly tyrosine-phosphorylates STAT5 on its activation site and is involved in
965 erythropoietin-induced signaling pathway. *Oncogene*. 2001;20:6643-6650. doi:
966 10.1038/sj.onc.1204807
967 26. Wingelhofer B, Neubauer HA, Valent P, Han X, Constantinescu SN, Gunning PT, Muller
968 M, Moriggl R. Implications of STAT3 and STAT5 signaling on gene regulation and
969 chromatin remodeling in hematopoietic cancer. *Leukemia*. 2018;32:1713-1726. doi:
970 10.1038/s41375-018-0117-x
971 27. Gu L, Liao Z, Hoang DT, Dagvadorj A, Gupta S, Blackmon S, Ellsworth E, Talati P, Leiby
972 B, Zinda M, et al. Pharmacologic inhibition of Jak2-Stat5 signaling By Jak2 inhibitor

973 AZD1480 potently suppresses growth of both primary and castrate-resistant prostate
974 cancer. *Clin Cancer Res*. 2013;19:5658-5674. doi: 10.1158/1078-0432.CCR-13-0422
975 28. Dieudonne FX, Severe N, Biosse-Duplan M, Weng JJ, Su Y, Marie PJ. Promotion of
976 osteoblast differentiation in mesenchymal cells through Cbl-mediated control of STAT5
977 activity. *Stem Cells*. 2013;31:1340-1349. doi: 10.1002/stem.1380
978 29. Cuevas RA, Chu CC, Moorhead WJ, 3rd, Wong R, Sultan I, St Hilaire C. Isolation of
979 Human Primary Valve Cells for In vitro Disease Modeling. *J Vis Exp*. 2021:e62439. doi:
980 10.3791/62439
981 30. Ducy P, Zhang R, Geoffroy V, Ridall AL, Karsenty G. Osf2/Cbfa1: a transcriptional
982 activator of osteoblast differentiation. *Cell*. 1997;89:747-754. doi: 10.1016/s0092-
983 8674(00)80257-3
984 31. Otto F, Thornell AP, Crompton T, Denzel A, Gilmour KC, Rosewell IR, Stamp GW,
985 Beddington RS, Mundlos S, Olsen BR, et al. Cbfa1, a candidate gene for cleidocranial
986 dysplasia syndrome, is essential for osteoblast differentiation and bone development.
987 *Cell*. 1997;89:765-771. doi: 10.1016/s0092-8674(00)80259-7
988 32. Sun Y, Byon CH, Yuan K, Chen J, Mao X, Heath JM, Javed A, Zhang K, Anderson PG,
989 Chen Y. Smooth muscle cell-specific runx2 deficiency inhibits vascular calcification. *Circ*
990 *Res*. 2012;111:543-552. doi: 10.1161/CIRCRESAHA.112.267237
991 33. Lin ME, Chen T, Leaf EM, Speer MY, Giachelli CM. Runx2 Expression in Smooth
992 Muscle Cells Is Required for Arterial Medial Calcification in Mice. *Am J Pathol*.
993 2015;185:1958-1969. doi: 10.1016/j.ajpath.2015.03.020
994 34. Parra-Izquierdo I, Castanos-Mollor I, Lopez J, Gomez C, San Roman JA, Sanchez
995 Crespo M, Garcia-Rodriguez C. Calcification Induced by Type I Interferon in Human
996 Aortic Valve Interstitial Cells Is Larger in Males and Blunted by a Janus Kinase Inhibitor.
997 *Arterioscler Thromb Vasc Biol*. 2018;38:2148-2159. doi: 10.1161/ATVBAHA.118.311504
998 35. Parra-Izquierdo I, Castanos-Mollor I, Lopez J, Gomez C, San Roman JA, Sanchez
999 Crespo M, Garcia-Rodriguez C. Lipopolysaccharide and interferon-gamma team up to
1000 activate HIF-1alpha via STAT1 in normoxia and exhibit sex differences in human aortic
1001 valve interstitial cells. *Biochim Biophys Acta Mol Basis Dis*. 2019;1865:2168-2179. doi:
1002 10.1016/j.bbadis.2019.04.014
1003 36. Jin H, St Hilaire C, Huang Y, Yang D, Dmitrieva NI, Negro A, Schwartzbeck R, Liu Y, Yu
1004 Z, Walts A, et al. Increased activity of TNAP compensates for reduced adenosine

1005 production and promotes ectopic calcification in the genetic disease ACDC. *Sci Signal*.
1006 2016;9:ra121. doi: 10.1126/scisignal.aaf9109
1007 37. Moorhead WJ, 3rd, Chu CC, Cuevas RA, Callahan Jt, Wong R, Regan C, Boufford CK,
1008 Sur S, Liu M, Gomez D, et al. Dysregulation of FOXO1 (Forkhead Box O1 Protein)
1009 Drives Calcification in Arterial Calcification due to Deficiency of CD73 and Is Present in
1010 Peripheral Artery Disease. *Arterioscler Thromb Vasc Biol*. 2020;40:1680-1694. doi:
1011 10.1161/ATVBAHA.119.313765
1012 38. Jung JJ, Razavian M, Kim HY, Ye Y, Golestani R, Toczek J, Zhang J, Sadeghi MM.
1013 Matrix metalloproteinase inhibitor, doxycycline and progression of calcific aortic valve
1014 disease in hyperlipidemic mice. *Sci Rep*. 2016;6:32659. doi: 10.1038/srep32659
1015 39. Millan A, Lanzer P, Sorribas V. The Thermodynamics of Medial Vascular Calcification.
1016 *Front Cell Dev Biol*. 2021;9:633465. doi: 10.3389/fcell.2021.633465
1017 40. Kim NW, Piatyszek MA, Prowse KR, Harley CB, West MD, Ho PL, Coviello GM, Wright
1018 WE, Weinrich SL, Shay JW. Specific association of human telomerase activity with
1019 immortal cells and cancer. *Science*. 1994;266:2011-2015. doi: 10.1126/science.7605428
1020 41. Hao LY, Armanios M, Strong MA, Karim B, Feldser DM, Huso D, Greider CW. Short
1021 telomeres, even in the presence of telomerase, limit tissue renewal capacity. *Cell*.
1022 2005;123:1121-1131. doi: 10.1016/j.cell.2005.11.020
1023 42. Jin HY, Weir-McCall JR, Leipsic JA, Son JW, Sellers SL, Shao M, Blanke P, Ahmadi A,
1024 Hadamitzky M, Kim YJ, et al. The Relationship Between Coronary Calcification and the
1025 Natural History of Coronary Artery Disease. *JACC Cardiovasc Imaging*. 2021;14:233-
1026 242. doi: 10.1016/j.jcmg.2020.08.036
1027 43. Ogawa D, Nomiyama T, Nakamachi T, Heywood EB, Stone JF, Berger JP, Law RE,
1028 Bruemmer D. Activation of peroxisome proliferator-activated receptor gamma
1029 suppresses telomerase activity in vascular smooth muscle cells. *Circ Res*. 2006;98:e50-
1030 59. doi: 10.1161/01.RES.0000218271.93076.c3
1031 44. Chiang YJ, Hemann MT, Hathcock KS, Tessarollo L, Feigenbaum L, Hahn WC, Hodes
1032 RJ. Expression of telomerase RNA template, but not telomerase reverse transcriptase,
1033 is limiting for telomere length maintenance in vivo. *Mol Cell Biol*. 2004;24:7024-7031.
1034 doi: 10.1128/MCB.24.16.7024-7031.2004
1035 45. Tani T, Orimo H, Shimizu A, Tsuruoka S. Development of a novel chronic kidney
1036 disease mouse model to evaluate the progression of hyperphosphatemia and associated
1037 mineral bone disease. *Sci Rep*. 2017;7:2233. doi: 10.1038/s41598-017-02351-6

1038 46. Roake CM, Artandi SE. Regulation of human telomerase in homeostasis and disease.
1039 *Nat Rev Mol Cell Biol*. 2020;21:384-397. doi: 10.1038/s41580-020-0234-z
1040 47. Feng J, Funk WD, Wang SS, Weinrich SL, Avilion AA, Chiu CP, Adams RR, Chang E,
1041 Allsopp RC, Yu J, et al. The RNA component of human telomerase. *Science*.
1042 1995;269:1236-1241. doi: 10.1126/science.7544491
1043 48. Pascolo E, Wenz C, Lingner J, Hauel N, Priepke H, Kauffmann I, Garin-Chesa P, Rettig
1044 WJ, Damm K, Schnapp A. Mechanism of human telomerase inhibition by BIBR1532, a
1045 synthetic, non-nucleosidic drug candidate. *J Biol Chem*. 2002;277:15566-15572. doi:
1046 10.1074/jbc.M201266200
1047 49. Ghosh A, Saginc G, Leow SC, Khattar E, Shin EM, Yan TD, Wong M, Zhang Z, Li G,
1048 Sung WK, et al. Telomerase directly regulates NF-kappaB-dependent transcription. *Nat*
1049 *Cell Biol*. 2012;14:1270-1281. doi: 10.1038/ncb2621
1050 50. Liu N, Ding D, Hao W, Yang F, Wu X, Wang M, Xu X, Ju Z, Liu JP, Song Z, et al. hTERT
1051 promotes tumor angiogenesis by activating VEGF via interactions with the Sp1
1052 transcription factor. *Nucleic Acids Res*. 2016;44:8693-8703. doi: 10.1093/nar/gkw549
1053 51. Lee C, Huang CH. LASAGNA: a novel algorithm for transcription factor binding site
1054 alignment. *BMC Bioinformatics*. 2013;14:108. doi: 10.1186/1471-2105-14-108
1055 52. Wingender E, Dietze P, Karas H, Knuppel R. TRANSFAC: a database on transcription
1056 factors and their DNA binding sites. *Nucleic Acids Res*. 1996;24:238-241. doi:
1057 10.1093/nar/24.1.238
1058 53. Babu AN, Meng X, Zou N, Yang X, Wang M, Song Y, Cleveland JC, Weyant M,
1059 Banerjee A, Fullerton DA. Lipopolysaccharide stimulation of human aortic valve
1060 interstitial cells activates inflammation and osteogenesis. *Ann Thorac Surg*. 2008;86:71-
1061 76. doi: 10.1016/j.athoracsur.2008.03.008
1062 54. Natarajan K, Muller-Klieser D, Rubner S, Berg T. Stafia-1: a STAT5a-Selective Inhibitor
1063 Developed via Docking-Based Screening of in Silico O-Phosphorylated Fragments.
1064 *Chemistry*. 2020;26:148-154. doi: 10.1002/chem.201904147
1065 55. Elumalai N, Berg A, Natarajan K, Scharow A, Berg T. Nanomolar inhibitors of the
1066 transcription factor STAT5b with high selectivity over STAT5a. *Angew Chem Int Ed Engl*.
1067 2015;54:4758-4763. doi: 10.1002/anie.201410672
1068 56. Fredriksson S, Gullberg M, Jarvius J, Olsson C, Pietras K, Gustafsdottir SM, Ostman A,
1069 Landegren U. Protein detection using proximity-dependent DNA ligation assays. *Nat*
1070 *Biotechnol*. 2002;20:473-477. doi: 10.1038/nbt0502-473

1071 57. Gillis AJ, Schuller AP, Skordalakes E. Structure of the Tribolium castaneum telomerase
1072 catalytic subunit TERT. *Nature*. 2008;455:633-637. doi: 10.1038/nature07283
1073 58. Neculai D, Neculai AM, Verrier S, Straub K, Klumpp K, Pfitzner E, Becker S. Structure of
1074 the unphosphorylated STAT5a dimer. *J Biol Chem*. 2005;280:40782-40787. doi:
1075 10.1074/jbc.M507682200
1076 59. Jumper J, Evans R, Pritzel A, Green T, Figurnov M, Ronneberger O, Tunyasuvunakool
1077 K, Bates R, Zidek A, Potapenko A, et al. Highly accurate protein structure prediction with
1078 AlphaFold. *Nature*. 2021;596:583-589. doi: 10.1038/s41586-021-03819-2
1079 60. Yan Y, Tao H, He J, Huang SY. The HDOCK server for integrated protein-protein
1080 docking. *Nat Protoc*. 2020;15:1829-1852. doi: 10.1038/s41596-020-0312-x
1081 61. Tebo AG, Gautier A. A split fluorescent reporter with rapid and reversible
1082 complementation. *Nat Commun*. 2019;10:2822. doi: 10.1038/s41467-019-10855-0
1083 62. Liu JC, Lengner CJ, Gaur T, Lou Y, Hussain S, Jones MD, Borodic B, Colby JL,
1084 Steinman HA, van Wijnen AJ, et al. Runx2 protein expression utilizes the Runx2 P1
1085 promoter to establish osteoprogenitor cell number for normal bone formation. *J Biol*
1086 *Chem*. 2011;286:30057-30070. doi: 10.1074/jbc.M111.241505
1087 63. Stock M, Otto F. Control of RUNX2 isoform expression: the role of promoters and
1088 enhancers. *J Cell Biochem*. 2005;95:506-517. doi: 10.1002/jcb.20471
1089 64. Zhang S, Xiao Z, Luo J, He N, Mahlios J, Quarles LD. Dose-dependent effects of Runx2
1090 on bone development. *J Bone Miner Res*. 2009;24:1889-1904. doi: 10.1359/jbmr.090502
1091 65. Okura H, Sato S, Kishikawa S, Kaneto S, Nakashima T, Yoshida N, Takayanagi H,
1092 Kiyono H. Runx2-I isoform contributes to fetal bone formation even in the absence of
1093 specific N-terminal amino acids. *PLoS One*. 2014;9:e108294. doi:
1094 10.1371/journal.pone.0108294
1095 66. Banerjee C, Javed A, Choi JY, Green J, Rosen V, van Wijnen AJ, Stein JL, Lian JB,
1096 Stein GS. Differential regulation of the two principal Runx2/Cbfa1 n-terminal isoforms in
1097 response to bone morphogenetic protein-2 during development of the osteoblast
1098 phenotype. *Endocrinology*. 2001;142:4026-4039. doi: 10.1210/endo.142.9.8367
1099 67. Maida Y, Yasukawa M, Okamoto N, Ohka S, Kinoshita K, Totoki Y, Ito TK, Minamino T,
1100 Nakamura H, Yamaguchi S, et al. Involvement of telomerase reverse transcriptase in
1101 heterochromatin maintenance. *Mol Cell Biol*. 2014;34:1576-1593. doi:
1102 10.1128/MCB.00093-14

1103 68. Okamoto N, Yasukawa M, Nguyen C, Kasim V, Maida Y, Possemato R, Shibata T, Ligon
1104 KL, Fukami K, Hahn WC, et al. Maintenance of tumor initiating cells of defined genetic
1105 composition by nucleostemin. *Proc Natl Acad Sci U S A*. 2011;108:20388-20393. doi:
1106 10.1073/pnas.1015171108
1107 69. Gizard F, Nomiyama T, Zhao Y, Findeisen HM, Heywood EB, Jones KL, Staels B,
1108 Bruemmer D. The PPARalpha/p16INK4a pathway inhibits vascular smooth muscle cell
1109 proliferation by repressing cell cycle-dependent telomerase activation. *Circ Res*.
1110 2008;103:1155-1163. doi: 10.1161/CIRCRESAHA.108.186205
1111 70. Slagboom PE, Droog S, Boomsma DI. Genetic determination of telomere size in
1112 humans: a twin study of three age groups. *Am J Hum Genet*. 1994;55:876-882.
1113 71. Brouilette S, Singh RK, Thompson JR, Goodall AH, Samani NJ. White cell telomere
1114 length and risk of premature myocardial infarction. *Arterioscler Thromb Vasc Biol*.
1115 2003;23:842-846. doi: 10.1161/01.ATV.0000067426.96344.32
1116 72. Samani NJ, Boultby R, Butler R, Thompson JR, Goodall AH. Telomere shortening in
1117 atherosclerosis. *Lancet*. 2001;358:472-473. doi: 10.1016/S0140-6736(01)05633-1
1118 73. Kurz DJ, Kloeckener-Gruissem B, Akhmedov A, Eberli FR, Buhler I, Berger W, Bertel O,
1119 Luscher TF. Degenerative aortic valve stenosis, but not coronary disease, is associated
1120 with shorter telomere length in the elderly. *Arterioscler Thromb Vasc Biol*. 2006;26:e114-
1121 117. doi: 10.1161/01.ATV.0000222961.24912.69
1122 74. Evans MA, Walsh K. Clonal hematopoiesis, somatic mosaicism, and age-associated
1123 disease. *Physiol Rev*. 2023;103:649-716. doi: 10.1152/physrev.00004.2022
1124 75. Huzen J, Peeters W, de Boer RA, Moll FL, Wong LS, Codd V, de Kleijn DP, de Smet BJ,
1125 van Veldhuisen DJ, Samani NJ, et al. Circulating leukocyte and carotid atherosclerotic
1126 plaque telomere length: interrelation, association with plaque characteristics, and
1127 restenosis after endarterectomy. *Arterioscler Thromb Vasc Biol*. 2011;31:1219-1225. doi:
1128 10.1161/ATVBAHA.110.217158
1129 76. Yutzey KE, Demer LL, Body SC, Huggins GS, Towler DA, Giachelli CM, Hofmann-
1130 Bowman MA, Mortlock DP, Rogers MB, Sadeghi MM, et al. Calcific aortic valve disease:
1131 a consensus summary from the Alliance of Investigators on Calcific Aortic Valve
1132 Disease. *Arterioscler Thromb Vasc Biol*. 2014;34:2387-2393. doi:
1133 10.1161/ATVBAHA.114.302523

1134 77. Hoerstrup SP, Kadner A, Melnitchouk S, Trojan A, Eid K, Tracy J, Sodian R, Visjager JF,
1135 Kolb SA, Grunenfelder J, et al. Tissue engineering of functional trileaflet heart valves
1136 from human marrow stromal cells. *Circulation*. 2002;106:I143-150.
1137 78. Hortells L, Sur S, St Hilaire C. Cell Phenotype Transitions in Cardiovascular
1138 Calcification. *Front Cardiovasc Med*. 2018;5:27. doi: 10.3389/fcvm.2018.00027
1139 79. Bogdanova M, Zabirnyk A, Malashicheva A, Enayati KZ, Karlsen TA, Kaljusto ML,
1140 Kvitting JP, Dissen E, Sullivan GJ, Kostareva A, et al. Interstitial cells in calcified aortic
1141 valves have reduced differentiation potential and stem cell-like properties. *Sci Rep*.
1142 2019;9:12934. doi: 10.1038/s41598-019-49016-0
1143 80. Xu K, Xie S, Huang Y, Zhou T, Liu M, Zhu P, Wang C, Shi J, Li F, Sellke FW, et al. Cell-
1144 Type Transcriptome Atlas of Human Aortic Valves Reveal Cell Heterogeneity and
1145 Endothelial to Mesenchymal Transition Involved in Calcific Aortic Valve Disease.
1146 *Arterioscler Thromb Vasc Biol*. 2020;40:2910-2921. doi: 10.1161/ATVBAHA.120.314789
1147 81. Lindroos M, Kupari M, Heikkila J, Tilvis R. Prevalence of aortic valve abnormalities in the
1148 elderly: an echocardiographic study of a random population sample. *J Am Coll Cardiol*.
1149 1993;21:1220-1225. doi: 10.1016/0735-1097(93)90249-z
1150 82. Joung YH, Lim EJ, Darvin P, Chung SC, Jang JW, Do Park K, Lee HK, Kim HS, Park T,
1151 Yang YM. MSM enhances GH signaling via the Jak2/STAT5b pathway in osteoblast-like
1152 cells and osteoblast differentiation through the activation of STAT5b in MSCs. *PLoS*
1153 *One*. 2012;7:e47477. doi: 10.1371/journal.pone.0047477
1154 83. Lee KM, Park KH, Hwang JS, Lee M, Yoon DS, Ryu HA, Jung HS, Park KW, Kim J,
1155 Park SW, et al. Inhibition of STAT5A promotes osteogenesis by DLX5 regulation. *Cell*
1156 *Death Dis*. 2018;9:1136. doi: 10.1038/s41419-018-1184-7
1157 84. Paulson M, Pisharody S, Pan L, Guadagno S, Mui AL, Levy DE. Stat protein
1158 transactivation domains recruit p300/CBP through widely divergent sequences. *J Biol*
1159 *Chem*. 1999;274:25343-25349. doi: 10.1074/jbc.274.36.25343
1160 85. Martino A, Holmes JHt, Lord JD, Moon JJ, Nelson BH. Stat5 and Sp1 regulate
1161 transcription of the cyclin D2 gene in response to IL-2. *J Immunol*. 2001;166:1723-1729.
1162 doi: 10.4049/jimmunol.166.3.1723
1163 86. Bergad PL, Towle HC, Berry SA. Yin-yang 1 and glucocorticoid receptor participate in
1164 the Stat5-mediated growth hormone response of the serine protease inhibitor 2.1 gene.
1165 *J Biol Chem*. 2000;275:8114-8120. doi: 10.1074/jbc.275.11.8114

1166 87. Yamada O, Ozaki K, Furukawa T, Machida M, Wang YH, Motoji T, Mitsuishi T, Akiyama
1167 M, Yamada H, Kawauchi K, et al. Activation of STAT5 confers imatinib resistance on
1168 leukemic cells through the transcription of TERT and MDR1. *Cell Signal*. 2011;23:1119-
1169 1127. doi: 10.1016/j.cellsig.2011.02.005
1170 88. Yamada O, Ozaki K, Akiyama M, Kawauchi K. JAK-STAT and JAK-PI3K-mTORC1
1171 pathways regulate telomerase transcriptionally and posttranslationally in ATL cells. *Mol*
1172 *Cancer Ther*. 2012;11:1112-1121. doi: 10.1158/1535-7163.MCT-11-0850
1173 89. Tormo AJ, Letellier MC, Sharma M, Elson G, Crabe S, Gauchat JF. IL-6 activates
1174 STAT5 in T cells. *Cytokine*. 2012;60:575-582. doi: 10.1016/j.cyto.2012.07.002
1175 90. Tanabe Y, Nishibori T, Su L, Arduini RM, Baker DP, David M. Cutting edge: role of
1176 STAT1, STAT3, and STAT5 in IFN-alpha beta responses in T lymphocytes. *J Immunol*.
1177 2005;174:609-613. doi: 10.4049/jimmunol.174.2.609
1178 91. Honda S, Miyamoto T, Watanabe T, Narumi T, Kadowaki S, Honda Y, Otaki Y,
1179 Hasegawa H, Netsu S, Funayama A, et al. A novel mouse model of aortic valve stenosis
1180 induced by direct wire injury. *Arterioscler Thromb Vasc Biol*. 2014;34:270-278. doi:
1181 10.1161/ATVBAHA.113.302610
1182 92. Sider KL, Blaser MC, Simmons CA. Animal models of calcific aortic valve disease. *Int J*
1183 *Inflam*. 2011;2011:364310. doi: 10.4061/2011/364310
1184 93. Balani K, Brito FC, Kos L, Agarwal A. Melanocyte pigmentation stiffens murine cardiac
1185 tricuspid valve leaflet. *J R Soc Interface*. 2009;6:1097-1102. doi: 10.1098/rsif.2009.0174
1186 94. Carneiro F, Kruithof BP, Balani K, Agarwal A, Gaussin V, Kos L. Relationships between
1187 melanocytes, mechanical properties and extracellular matrix composition in mouse heart
1188 valves. *J Long Term Eff Med Implants*. 2015;25:17-26. doi:
1189 10.1615/jlongtermeffmedimplants.2015011748
1190 95. Mjaatvedt CH, Kern CB, Norris RA, Fairey S, Cave CL. Normal distribution of
1191 melanocytes in the mouse heart. *Anat Rec A Discov Mol Cell Evol Biol*. 2005;285:748-
1192 757. doi: 10.1002/ar.a.20210
1193 96. Dharmarajan S, Speer MY, Pierce K, Lally J, Leaf EM, Lin ME, Scatena M, Giachelli CM.
1194 Role of Runx2 in Calcific Aortic Valve Disease in Mouse Models. *Front Cardiovasc Med*.
1195 2021;8:687210. doi: 10.3389/fcvm.2021.687210
1196 97. Lanzer P, Hannan FM, Lanzer JD, Janzen J, Raggi P, Furniss D, Schuchardt M,
1197 Thakker R, Fok PW, Saez-Rodriguez J, et al. Medial Arterial Calcification: JACC State-

1198 of-the-Art Review. *J Am Coll Cardiol*. 2021;78:1145-1165. doi:
1199 10.1016/j.jacc.2021.06.049
1200

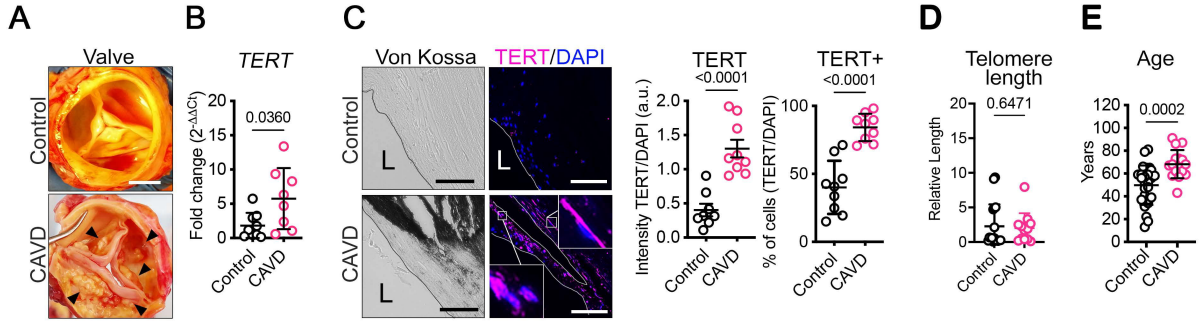

Figure 1. TERT is elevated in CAVD tissues. (**A**) Examples of non-calcified control (top) and calcified CAVD (bottom) human valves used in this study. Arrowheads indicate calcified nodules Scalebar. 1 cm. (**B**), *TERT* mRNA transcript quantification in control and CAVD valve tissues. n = 8 control, n= 9 CAVD. (**C**), Representative serial sections of Von Kossa (dark precipitation) and TERT immunofluorescent staining in control and CAVD valve tissues. Scalebar 100 µm. Graphs show the quantification of TERT intensity and the number of TERT-positive cells. n = 9 control, n = 9 CAVD. (**D**), Telomere length measurements in valve tissues. n = 19 control, n = 12 CAVD. (**E**), Age of the patients utilized in this study. n = 25 control, n = 16 CAVD. Data are shown as means ± SD. P values were calculated using the Mann-Whitney U test and shown on each graph. L = lumen.

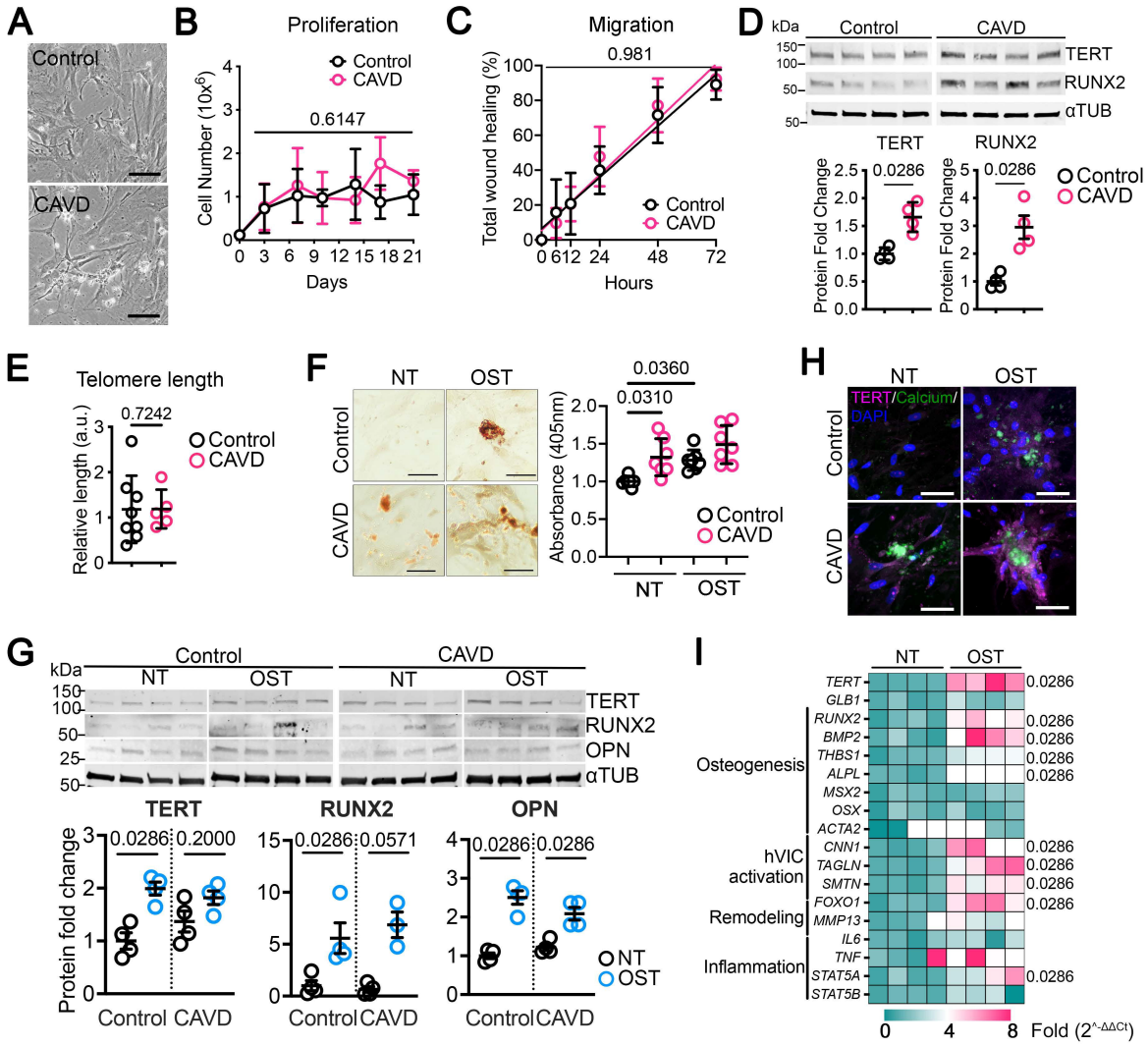

Figure 2. TERT is elevated in CAVD hVICs at baseline and upregulation during osteogenic reprogramming. (**A**), Representative images showing cell morphology of control and CAVD hVICs. Scalebar 50 µm. (**B**), Proliferation of control and CAVD hVICs at baseline. n = 3 both groups. (**C**) Relative migration distances of control and CAVD VICs. n = 10 both groups. (**D**) Western blot staining of control and CAVD hVICs at baseline. Quantification of protein levels is shown on the right panels. n = 4 both groups. (**E**) Telomere length measurements in VICs. n = 8, control, n = 5 CAVD. (**F**) Representative images of early calcification in hVICs growing in normal conditions (no treatment NT) or stimulated with osteogenic media (OST) for 14 days. Calcium deposition was visualized by Alizarin Red staining. Scalebar 50 µm. Quantification of calcification on the right graphs. n = 7 both groups. (**G**), Western blot staining of samples from control and CAVD hVICs after 14 days of NT or OST. Quantification of protein levels is shown on the bottom graphs. n = 4 both groups. (**H**), Representative immunofluorescent staining images of TERT in control and CAVD hVICs after 14 days of NT or OST. Calcium deposition was visualized with OsteoImage. Scalebar 100 µm. (**I**) Expression profile control VICs after 14 days of NT and OST treatment. n = 4 both groups. Data are shown as means ± SD. P values were calculated by 2-way ANOVA (Figure C), the Mann-Whitney U test (Figures B, D, E, G, and I), and the Kruskal-Wallis H test with Dunn post hoc test Figure F) and shown on each graph. * P = 0.0286 in Figure I.

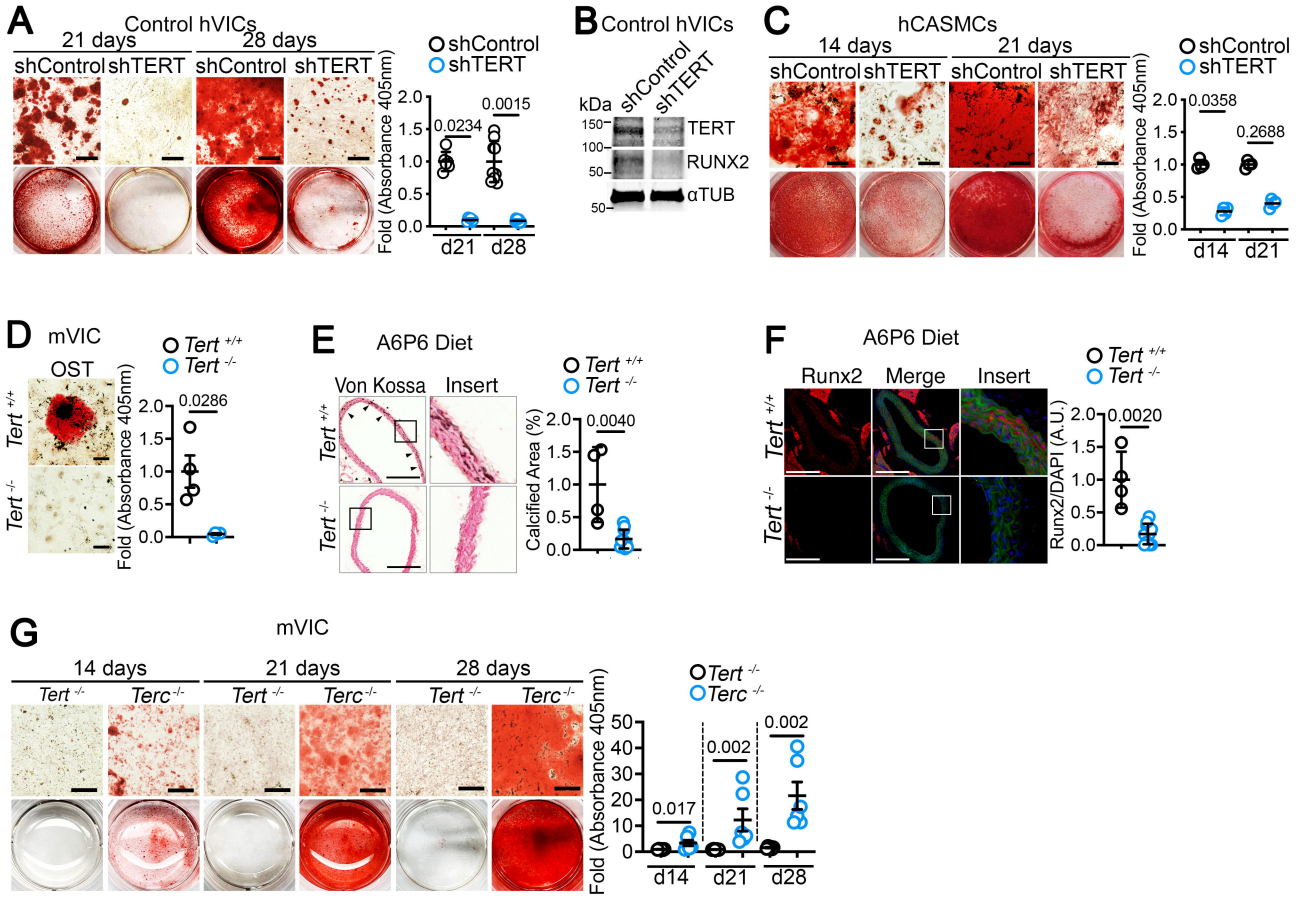

Figure 3. TERT is required to initiate osteogenic transition and calcify. (**A**) Control hVICs were transduced lentivirus containing shControl or shTERT and followed by OST stimulation for up to 28 days. Calcium deposition was visualized by Alizarin Red staining. n = 6 shControl, n = 6 shTERT at 21 days and n = 9 each group at day 28. Scalebar 400 µm. (**B**) Representative western blot staining of control hVICs transduced with lentivirus containing either shControl or shTERT followed by 7 days of OST. (**C**) hCASMCs were transduced with shControl or shTERT and stimulated with OST for 14 and 21 days. n = 4 for each group at both time points. Scalebar 400 µm. (**D**) Representative images of mVIC isolated from *Tert*$^{+/+}$ and *Tert*$^{-/-}$ mice were stimulated with OST for 28 days. Scalebar 400 µm. (**E**) Representative Von Kossa staining images of *Tert*$^{+/+}$ and *Tert*$^{-/-}$ mice aortas (dark precipitation). Scale bar 400 µm. Quantification of calcification is shown on the right panel. (**F**) Representative immunofluorescent images of Runx2 expression indicative of calcification (red, insert) on *Tert*$^{+/+}$ and *Tert*$^{-/-}$ mice aorta. Scale bar 400 µm. Runx2 quantification of calcification is shown on the right panel. (**G**) Representative images of mVICs isolated from F1 *Tert*$^{-/-}$ or *Terc*$^{-/-}$ mice were stimulated with OST for up to 21 days. Scalebar 100 µm. Data are shown as means ± SD. P values were calculated using the Kruskal-Wallis H test, Dunn post hoc test (Figures A, C, and G), and Mann-Whitney U test (Figures D, E, and F).

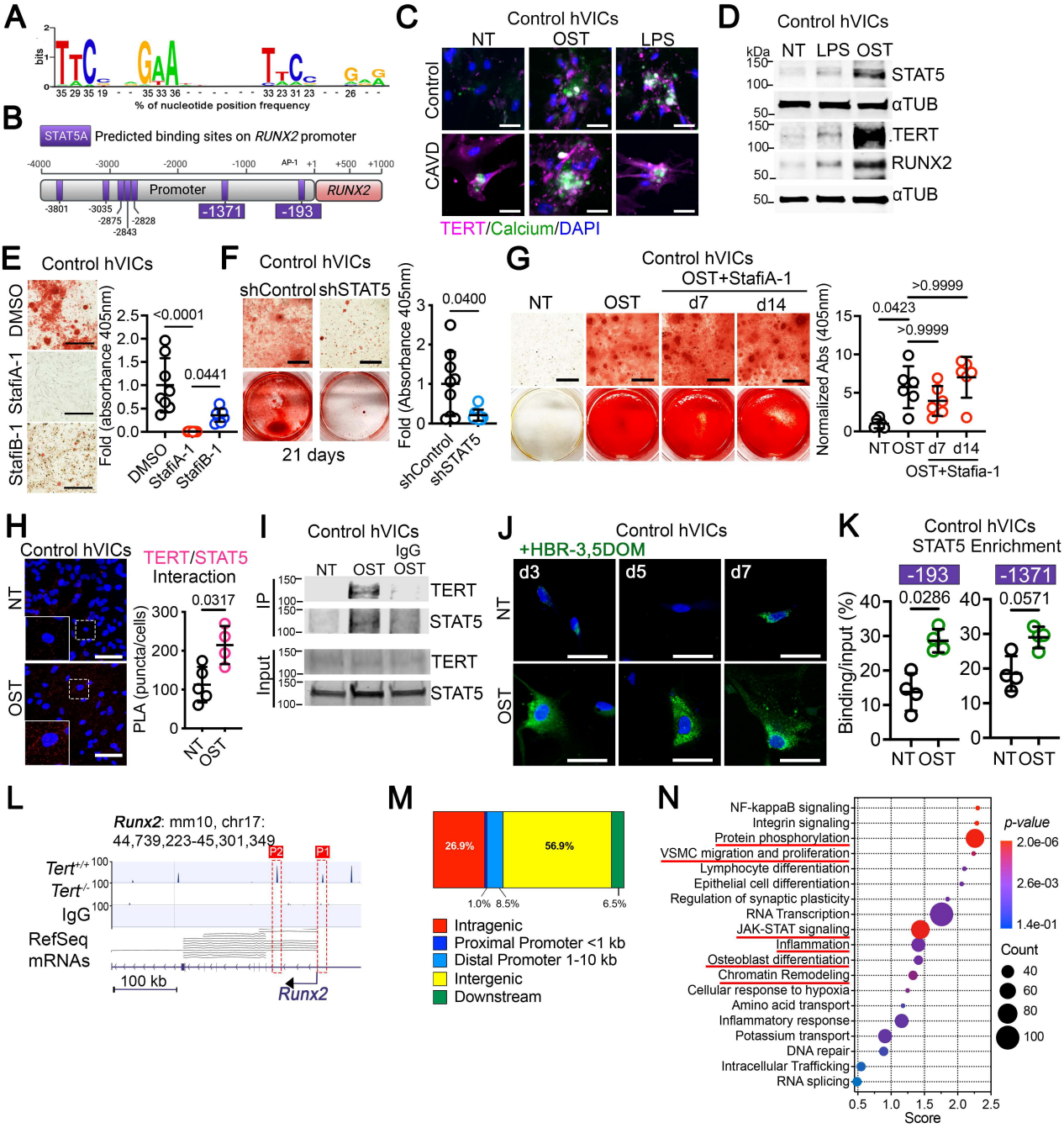

Figure 4. STAT5 binds to TERT and is required for the calcification of human VICs. (**A**) Graphic of in silico analysis identifying the consensus binding site for STAT5. (**B**), Diagram depicting STAT5 binding to RUNX2 promoter and the positions of the predicted STAT5 binding sites (purple boxes). (**C**) Representative immunofluorescence images of control hVICs after 14 days of LPS treatment or OST stimulation. Scalebar 50 μm. (**D**) Representative western blot staining of hVICs after 14 days of OST stimulation. (**E**) Representative images of control hVICs treated with 10 μM of the STAT5 inhibitors StafiA-1 or StafiB-1 throughout 28 days of osteogenic stimulation. Scalebar 400 μm. n = 8 each group. The quantification of calcification is shown on the right graph. (**F**) Control hVICs were transduced with lentivirus containing shControl or shSTAT5 constructs and treated with OST for 21 days. Calcium deposition was visualized by Alizarin Red staining. n = 9 for each group. Scalebar 400 μm. (**G**) Representative images of hVIC (left panels) treated with 10 μM of the STAT5 inhibitors StafiA-1 starting at d7 or d14 of OST treatment. Samples were collected at d21. Scalebar 400 μm. n = 6 for each group. (**H**) Representative images of TERT/STAT5 complex (red foci) in control hVICs cultured for 21 days in osteogenic medium and detected by PLA. Scalebar 100 μm. n = 4 for each group. (**I**) TERT/STAT5 interaction was detected by co-immunoprecipitation in control hVICs under OST for 21 days. (**J**) Control hVIC co-expressing TERT-NFAST and STAT5A-CFAST were labeled with 5 μM HBR-3,5DOM (4-hydroxy-3,5-dimethoxybenzylidene rhodamine, coral) and imaged at d3, d5, and d7 of osteogenic treatment (OST) or control no-treatment (NT). Scale bars 50 μm. (**K**) Chromatin immunoprecipitation shows enrichment of STAT5 on RUNX2 promoter OST conditions compared to NT. The base position is indicated in the blue boxes. n=4 for each group as in B. (**L**) STAT5 CUT&Tag sequencing tracks in genomic regions of Runx2 in no-treatment control and osteogenic condition-treated mice VICs. (**M**) Stacked chart representing genome-wide STAT5 occupancy in promoters, genes, and intergenic regions frequency in mice VICs. (**N**) Top 20 GO pathways enriched in genes with significant loss of STAT5 in *Tert*$^{+/+}$ vs *Tert*$^{-/-}$ mice VICs. Data are shown as means ± SD. P values were calculated by the Mann-Whitney U test (Figures F, H, and J) and the Kruskal-Wallis H test (Figures E and G) and indicated on top of each graph.

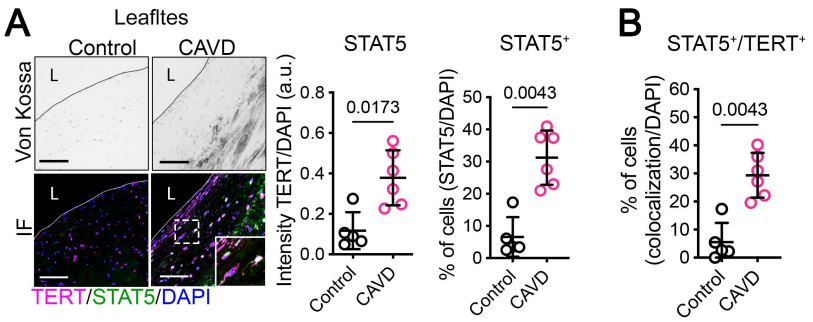

Figure 5. TERT and STAT5 are upregulated and colocalized in CAVD tissue. (**A**) Representative serial sections of Von Kossa (dark precipitation) and TERT and STAT5 immunofluorescent staining in control and CAVD tissues. Scalebar 100 µm. STAT5 intensity and STAT5-positive cells (STAT5+) are quantified on the right panels. (**B**) Quantification of STAT5-TERT-positive cells. Data are shown as means ± SD, n = 5 control, n = 6 CAVD. P values were calculated with the Mann-Whitney U test and indicated on each graph. L = lumen.

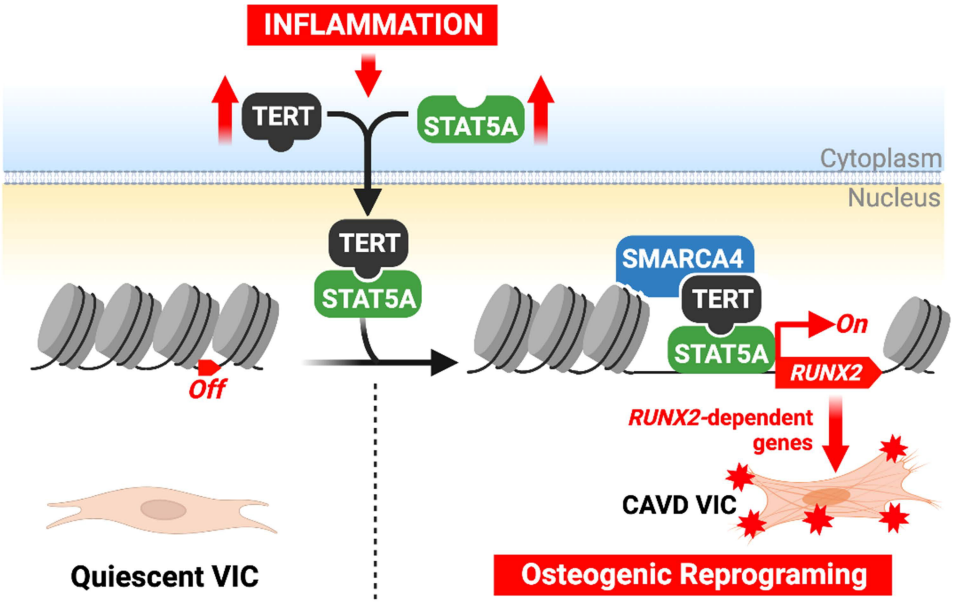

Figure 6. TERT/STAT5 promotes osteogenic reprogramming. Inflammatory signals promote the upregulation and interaction of TERT and STAT5A. The TERT/STAT5 complex translocates into the nucleus, where TERT interacts with SMARCA4 (also known as BRG1), which facilitates a permissive chromatin configuration, and STAT5A binds specific sites on the RUNX2 promoter, leading to the osteogenic reprogramming of valve interstitial cells during the early stages of CAVD pathogenesis.

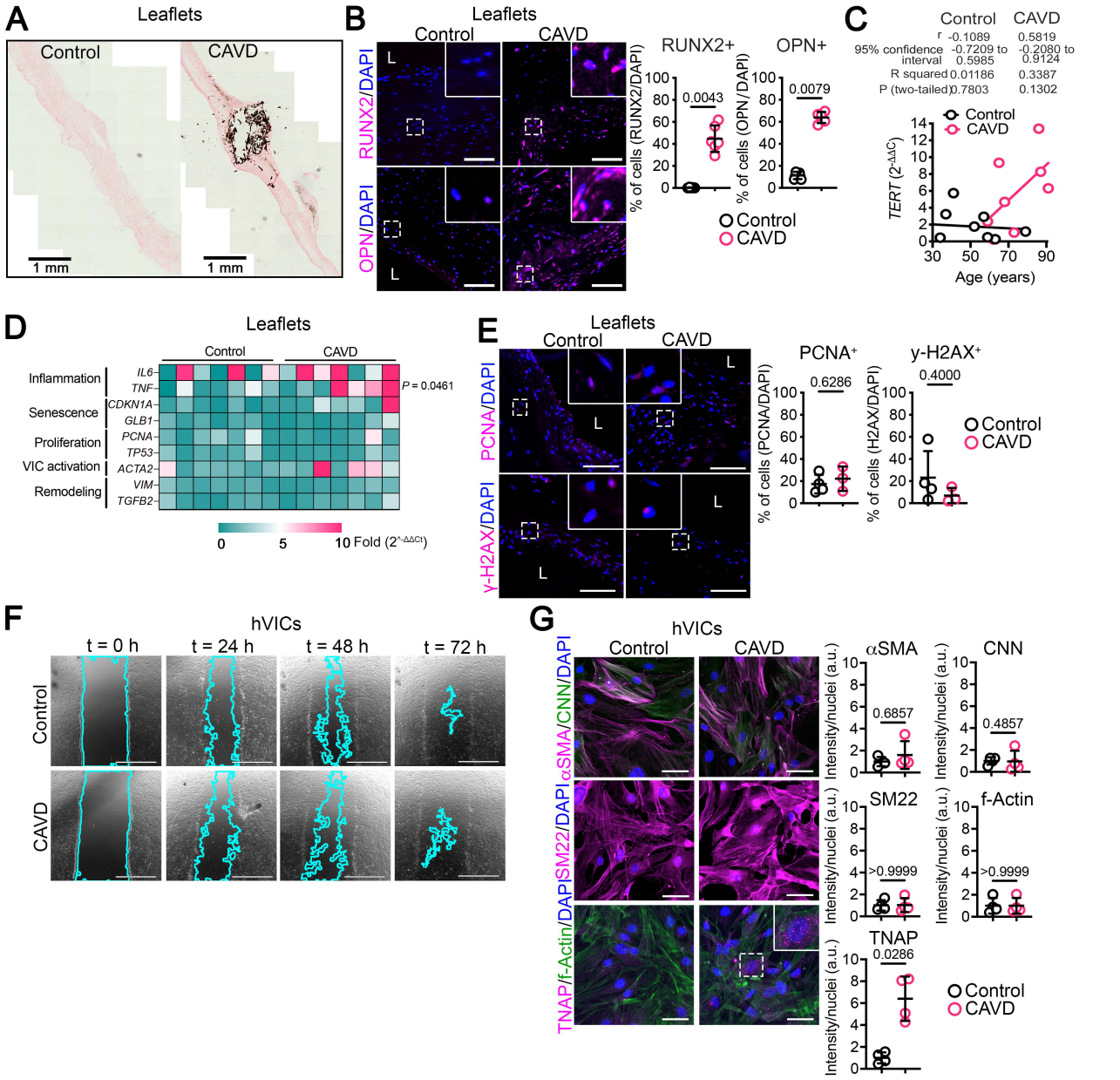

Supplemental Figure 1. Characterization of human CAVD valves and patient-isolated VICs at baseline. (**A**) Representative section of Von Kossa staining in control and valve CAVD leaflets tissue. Scalebar 1 mm. (**B**) Representative serial sections of RUNX2 immunofluorescent staining and OPN in control and CAVD valve tissues. Scalebar 100 μm. Quantification of RUNX2-positive cells and OPN-positive cells on the leaflet specimen is shown on the right graphs. n = 5 control, n = 6 CAVD. (**C**) Correlation between age of the donor and TERT expression in valve tissues. n = 8 control, n = 9 CAVD. (**D**) Gene expression profile in the valve leaflets. n = 7 each group. (**E**) Representative images of immunofluorescent staining of PCNA (top panels) and γ-H2AX (bottom panels) in control and CAVD valve tissues. Scalebar 100 μm. Quantification of PCNA-positive cells and γ-H2AX-positive cells are shown on the right graphs. n = 4 control, n = 3 CAVD. (**F**) Representative images of a scratch assay in control and CAVD hVICs. Time points are indicated on top of each panel. Blue lines denote the cell migration front. Scalebar 1 mm. n = 10 of each group. (**G**) Representative images of αSMA, CNN, SM22, TNAP, and f-Actin in control and CAVD hVICs. Scalebar 50 μm. Signal quantification is shown on the right. n = 4 each group. Data are shown as means ± SD. P values were calculated with the Mann-Whitney U test (Figures A, B, D, F, and G), Pearson correlation test (Figure C), and two-way ANOVA with the Sidak post hoc test (Figure D and shown on top of each graph). L = lumen.

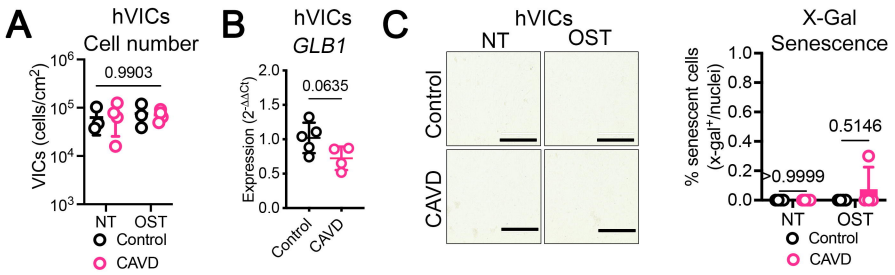

Supplemental Figure 2. Inhibition of reverse transcriptase activity of TERT does not prevent osteogenic reprogramming of hVICs. (**A**) Cell counts of control and CAVD hVICs after 14 days of NT or OST stimulation. n = 4 each group. (**B**) β-galactosidase (*BLG1*) mRNA transcript quantification in control and CAVD hVICs at baseline. n = 5 control, n= 4 CAVD. (**C**) Representative images of senescence-associated β-galactosidase activity staining of hVICs after 28 days of NT or OST stimulation. Blue cells were considered positive for senescence. Quantification of senescence is shown on the right graph. n = 4 each group. Data are shown as means ± SD. P values were calculated with the Mann-Whitney U test (Figure B) and the Kruskal-Wallis H test with Dunn pairwise comparison post hoc test (Figures A, C) and shown on top of each graph. Scalebar 400 µm. n = 6 for each group.

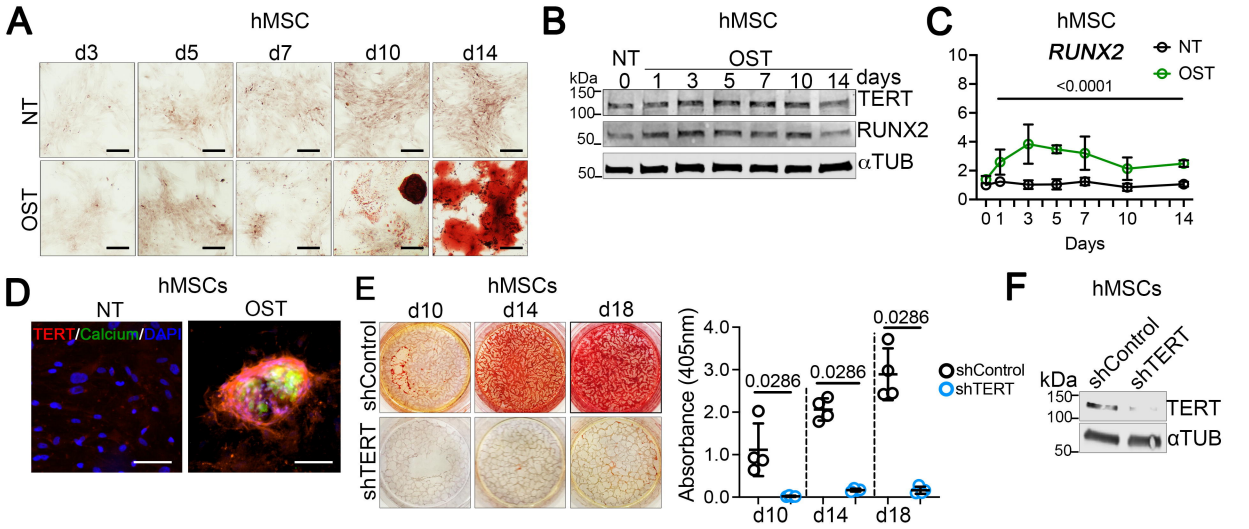

Supplemental Figure 3. TERT is upregulated and required for the osteogenic differentiation of human mesenchymal stem cells. (**A**) Representative images of hMSCs stimulated with OST for 14 days. Calcium deposition was visualized by Alizarin Red staining. Scalebar 50 µm. (**B**) Western blot staining of samples from hMSCs collected during the 14 days of OST treatment. (**C**) *RUNX2* expression profile of differentiating hMSCs stimulated for 14 days with OST media. n = 3. (**D**) Representative TERT immunofluorescent staining images of hMSCs stimulated with OST for 14 days. Scalebar 100 µm. (**E**) Representative images of hMSCs infected with shTERT or shControl virus and stimulated with OST for 14 days. Calcium deposition was visualized by Alizarin Red staining. The quantification of calcification is shown on the right graph. n = 3. (**F**) Western blot staining of samples from hMSCs collected during the 14 days of OST treatment. Data are shown as means ± SD. P values were calculated with the Kruskal-Wallis H test with Dunn pairwise comparison post hoc test (Figure C) and the Mann-Whitney U test (Figure E) and shown on each graph.

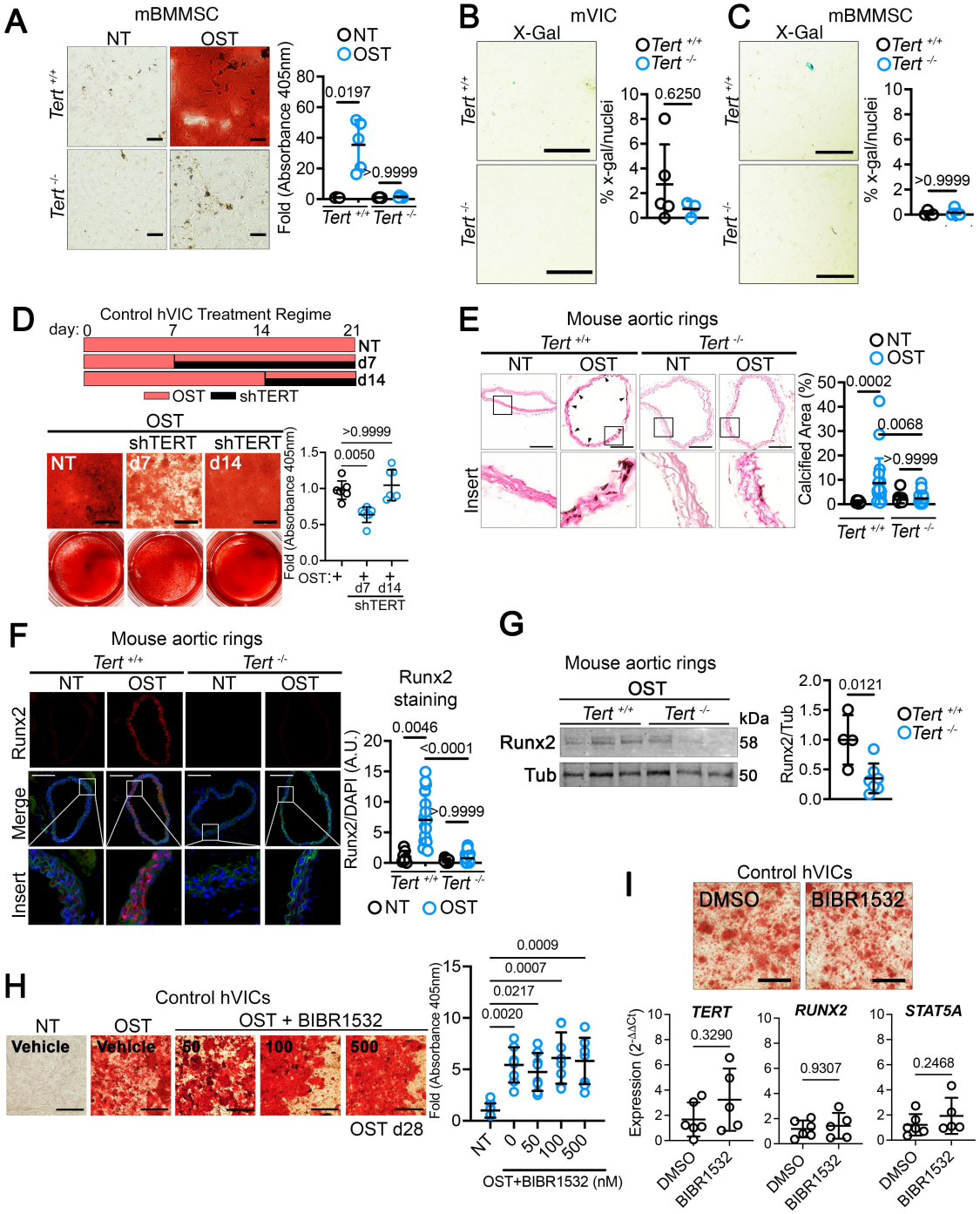

Supplemental Figure 4. Inhibition of reverse transcriptase activity of TERT does not prevent osteogenic reprogramming of VICs. (**A**) Representative images of mBMMSCs isolated from *Tert*$^{+/+}$ or *Tert*$^{-/-}$ mice and stimulated with OST for 21 days. Scalebar 100 µm. Quantification of calcification is presented as average absorbance on the right graphs, n = 5 for each group. (**B, C**) Representative images of a senescence-associated β-galactosidase (SA-β-gal) staining of mVICs and mBMMSCs isolated from *Tert*$^{+/+}$ or F1 *Tert*$^{-/-}$ mice after 21 days of OST stimulation. In each group, blue cells were considered positive for senescence, n = 5. (**D**) Schematic of OST treatment with delayed shTERT transduction (top panel). VICs were transduced with shTERT, and calcification was assessed with Alizarin Red S stain at day 21. Scalebar 400 µm. n = 6 for each group. (**E**) Representative sections of Von Kossa staining in thoracic aortic rings isolated from *Tert*$^{+/+}$ and *Tert*$^{-/-}$ mice after 14 days of OST treatment relative to NT control treatment. Quantification is shown on the right. Scale bar 400 µm (**F**) Immunofluorescence staining of thoracic aortic rings after OST treatment as in B. Quantification of Runx2 is shown on the right graph. Scale bar 400 µm (**G**) Western blot staining of aortic ring specimens collected and treated in B. Quantification of Runx2 is shown on the right graph. (**H**) Human VICs were treated with the TERT inhibitor BiBR1532 and stimulated with OST, and calcification was assessed on day 28, with n = 5 in each group. (**I**) *TERT*, *RUNX2*, and *STAT5A* expression were evaluated on day 14, n = 6 DMSO, n = 5 BIBR1532. Data are shown as means ± SD. P values were calculated with the Kruskal-Wallis H test with Dunn pairwise comparison post hoc test (Figures A, B, C, E, H) and the Mann-Whitney U test (Figures D, F, G, I) and are shown on top of each graph.

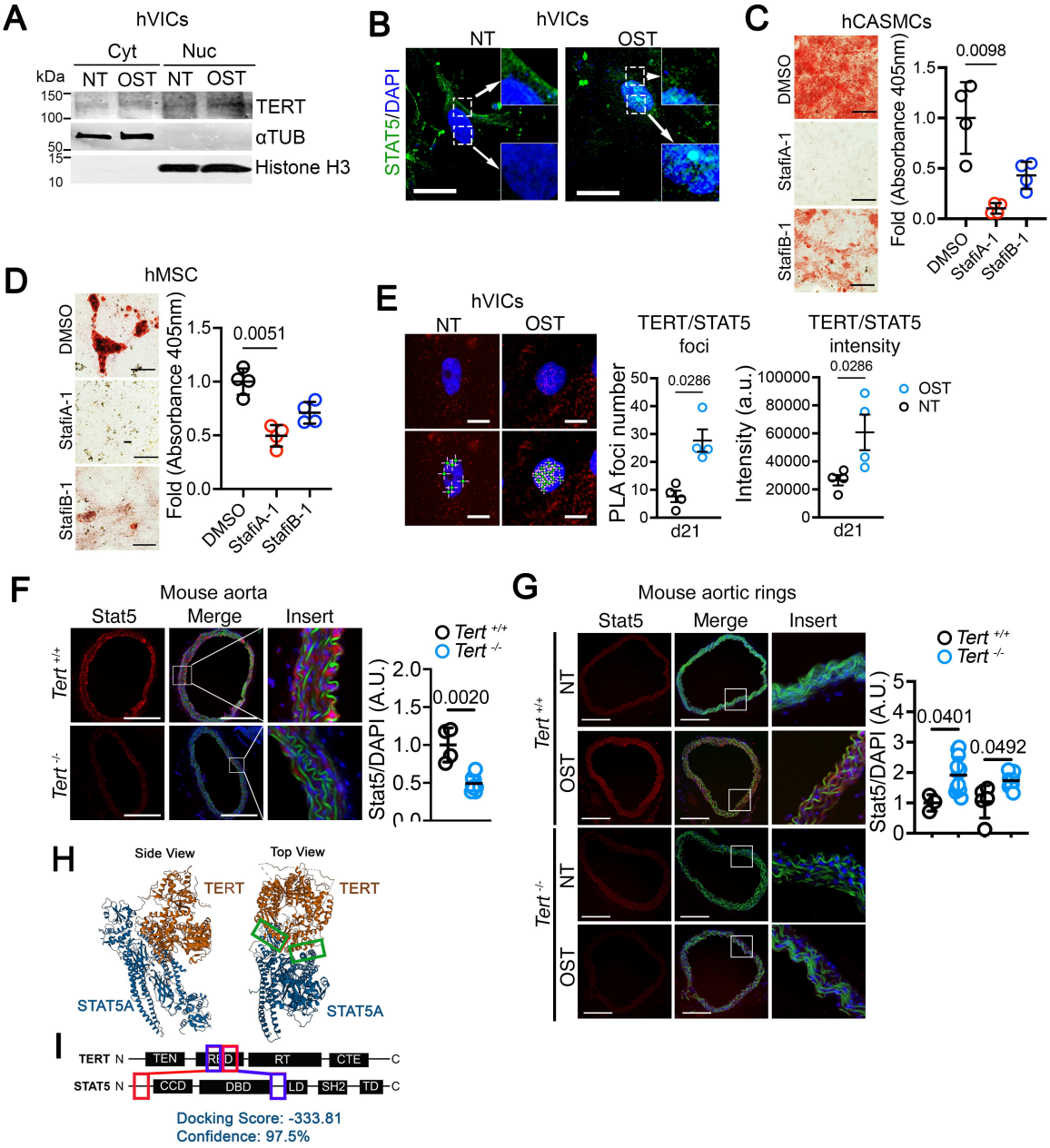

Supplemental Figure 5. STAT5 is upregulated, binds to TERT, and is required for osteogenic reprogramming of VICs. (**A**) Western blot analysis of cytoplasmic and nuclear fractions of TERT from control VICs obtained after seven days of OST stimulation. Fractions purity was assessed by staining for markers of cytoplasm (TUB) and nucleoplasm (Histone H3). Cyt, cytoplasmic fraction; Nuc, nuclear fraction. (**B**) Representative immunofluorescence image of STAT5 shows subcellular distribution after 14 days of NT and OST stimulation. Scalebar 40 µm. (**C**) Representative images of CASMCs treated with 10 µM of the STAT5 inhibitors StafiA-1 or StafiB-1 during the 14 days of OST stimulation. Scalebar 400 µm. n = 4 for each group. (**D**) Representative images of MSCs treated with 10 µM of the STAT5 inhibitors StafiA-1 or StafiB-1 during the 21 days of OST stimulation. Scalebar 400 µm. n = 4 for each group. (**E**) Representative images of TERT/STAT5 complex (red foci) detected by proximity ligation assay (PLA) in the nucleus of control VICs. Scalebar 25 µm. The PLA foci quantification and intensity are shown on the right graph. n = 4 for each group. (**H**) Mol*3D Viewer rendering of the TERT-STAT5 dimer interaction predicted by the HDock. Red boxes indicate the position of the interaction between TERT and STAT5. (**F**) Representative immunofluorescent images of Stat5 expression after 12 weeks of high adenine high phosphate diet on *Tert*$^{-/-}$ *and Tert*$^{-/-}$ mice aorta. Scale bar 400 µm. Quantification of Stat5 expression is shown on the right panel. (**G**) Representative images of Stat5 immunofluorescence staining of thoracic aortic rings isolated from *Tert*$^{+/+}$ and *Tert*$^{-/-}$ mice after 14 days of OST treatment relative to NT control treatment. Quantification of Stat5 is shown on the right graph. Scale bar 400 µm (**I**) The diagram shows the regions involved in the predicted interaction as indicated in A, and the docking and confidence scores predicted by HDock are indicated. TEN: DNA anchor domain for processive telomeric repeat addition, RBD: Telomerase RNA binding domain, RT: Finger and palm region of the reverse transcriptase domain, CTE: C-terminal extension or putative thumb domain of the reverse transcriptase, CCD: Coiled-coil domain, required for nuclear localization, DBD: DNA binding domain, HLK: Helical linker and DNA binding domain, SH2: Domain required for activation and dimerization, TD: Transactivation domain. Data are shown as means ± SD. P values were calculated with the Mann-Whitney U test (Figures A and G) and the Kruskal-Wallis H test with Dunn pairwise comparison post-test (Figures B, E, and F) and indicated in each graph.

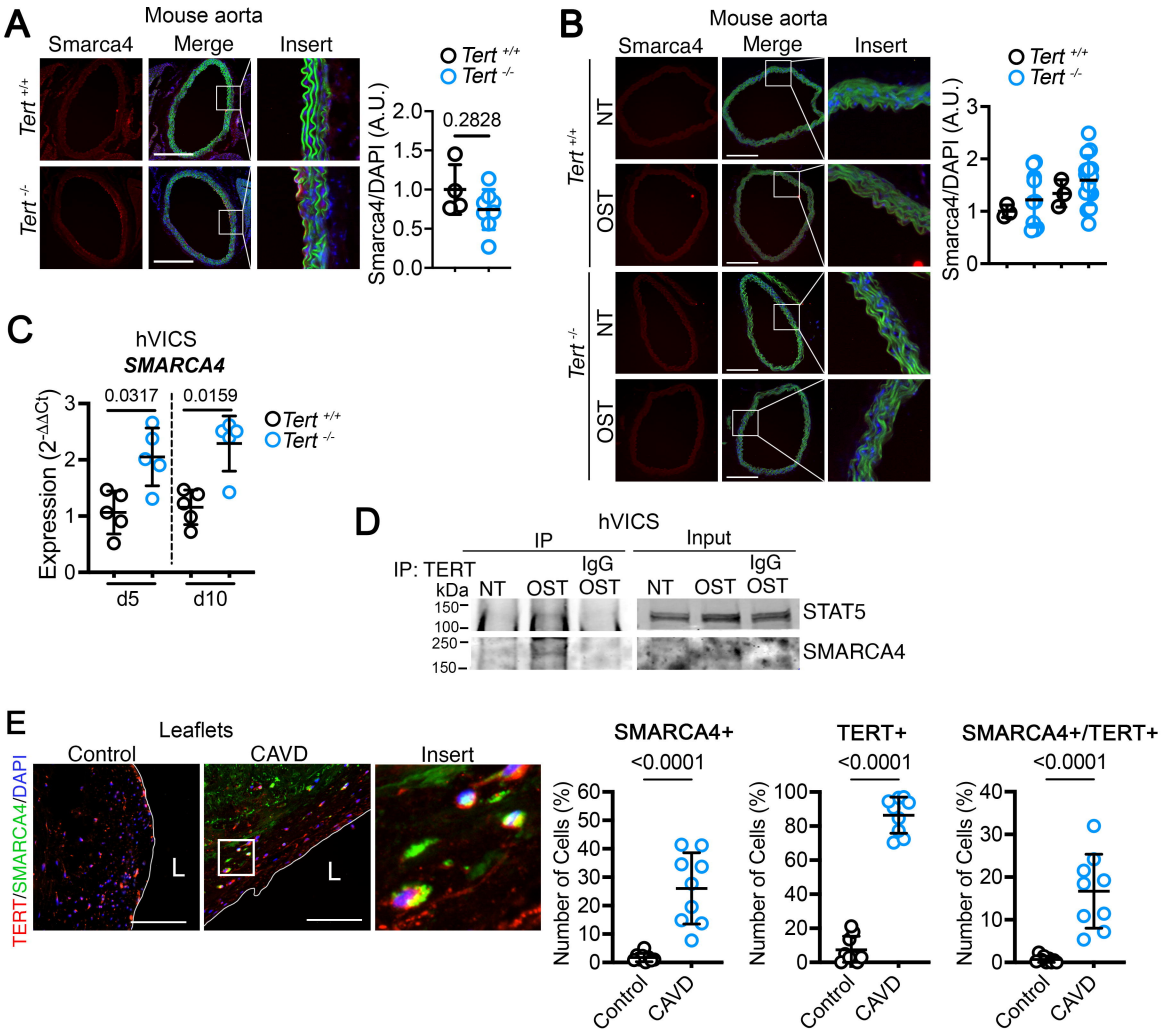

Supplemental Figure 6. Chromatin remodeling enzyme SMARCA4 is upregulated and interacts with TERT during the osteogenic reprogramming of VICs. (**A**) Representative immunofluorescent images of Smarca4 expression after 12 weeks of high adenine high phosphate diet on *Tert*$^{-/-}$ *and Tert*$^{-/-}$ mice aorta. Scale bar 400 µm. Quantification of Smarca4 expression is shown on the right panel. (**B**) Representative images of Smarca4 immunofluorescence staining of thoracic aortic rings isolated from *Tert*$^{+/+}$ and *Tert*$^{-/-}$ mice after 14 days of OST treatment relative to NT control treatment. Quantification of Smarca4 is shown on the right graph. (**C**) *SMARCA4* expression was evaluated on days 5 and 10 on VICs stimulated with OST. n = 5 each group. (**E**) TERT/STAT and TERT/SMARCA4 interaction was detected by co-immunoprecipitation upon osteogenic stimulation on VIC. (**E**) Representative TERT and SMARCA4 immunofluorescent staining in control and CAVD tissues. The number of positive cells is shown on the right graphs. n = 9 control, n = 9 CAVD. Scalebar 100 µm. Data are shown as means ± SD, and P values were calculated with the Mann-Whitney U test and indicated on each graph in Figures A and C. L = lumen.